



New palaeomagnetic data from metamorphosed carbonates of Western Oscar II Land, Western Spitsbergen

Krzysztof MICHALSKI ^{1*}, Krzysztof NEJBERT ², Justyna DOMAŃSKA-SIUDA ²
and Geoffrey MANBY ³

¹ Instytut Geofizyki, Polska Akademia Nauk, ul. Księcia Janusza 64,
01-452 Warszawa, Poland <krzysztof.michalski@igf.edu.pl>

² Wydział Geologii, Uniwersytet Warszawski, al. Żwirki i Wigury 93, 02-089 Warszawa, Poland
<knejbort@uw.edu.pl> <j.domanska@uw.edu.pl>

³ Natural History Museum of London, Great Britain, Cromwell Road, London, UK
<g.m.manby@btinternet.com>

* corresponding author

Abstract: Palaeomagnetic-petrographic-structural analyses of Proterozoic–Lower Palaeozoic metamorphosed carbonates from 12 locations within Oscar II Land (Western Spitsbergen) have been carried out to determine their usefulness in palaeogeographic reconstructions for Caledonian time. Structural analyses confirm that metacarbonates record several stages of deformation: D1, D2 ductile phases related to Caledonian metamorphism and a D3 brittle phase related to Late Cretaceous–Paleogene evolution of the West Spitsbergen Fold Belt. The latter is represented by thrust faults, localized folds with strain slip cleavages and late extensional collapse. Petrographic investigations reveal that Caledonian greenschist facies metamorphism was characterized by the high activity of H₂O–CO₂-rich fluids which promoted extensive recrystallization and within-rock spatial reorganization of sampled metacarbonates. Microscopic, SEM and microprobe analyses exclude the existence of any primary pre-metamorphic ferromagnetic minerals (primary-related to sedimentation and or early diagenesis) and point to metamorphic 4C superstructure (Fe₇S₈) pyrrhotite as the main ferromagnetic carrier in investigated rocks. This is confirmed by the three-component isothermal remanent magnetization (IRM) procedures and the results of thermal demagnetizations. In 12 sites a total number of 72 independently oriented palaeomagnetic samples were collected from which 181 specimens were drilled and thermally demagnetized. Sampled metacarbonates are weakly magnetized (NRM <0.2mA/m). The statistically significant palaeomagnetic results were achieved only from 1 of 12 investigated sites. In one site situated in the Western overturned limb of the Holmesletfjellet Syncline intermediate unblocking temperatures – “pyrrhotite related” component WTSJ5M superimposed on the S1 Caledonian schistosity was recognized (D = 100.7°, I = -21.4° α95% = 5.5°, κ = 58.23). Coincidence of WTSJ5M with Silurian–Devonian sector of the Baltica reference path after unfolding of the syncline by the angle of 130° suggests synfolding origin of this direction. Further, this suggests that Holmesletfjellet Syncline originated as an open fold and has been transformed into an overturned syncline during the Late Caledonian shortening or in the Late Cretaceous–Palaeogene time.

Key words: Arctic, Spitsbergen, Caledonides, West Spitsbergen Fold Belt, palaeomagnetism, petrography, metacarbonates, metamorphic pyrrhotite, ferromagnetic carriers.

Introduction

The Caledonian basement of Svalbard is divided into three main crustal units or terranes, which were assembled from widely disparate locations along the Eastern and the Northern margins of Greenland to Ellesmere Island in the Late Devonian time (Harland 1997; Harland and Wright 1979). Michalski *et al.* (2012) demonstrated, in contrast, that the amalgamation of the Central and Eastern Terranes took place not later than in the Silurian during the final Caledonian collision of Baltica and Laurentia. The origin and timing of final docking of the Western Terrane remains, however, controversial. This study focuses on the western part of Oscar II Land (Fig. 1), which according to Harland and Wright (1979) and Harland (1997), constitutes a part of the Western Terrane that is separated from the Central Terrane by Kongsfjorden-Hansbreen fault zone. Here, by integrating palaeomagnetic, structural and petrographic data from the metacarbonates of Oscar II Land an attempt is made to establish the palaeogeographic location of the Western Terrane in Caledonian time. The main aim here is to recognize the ferromagnetic carriers within the metacarbonates of the Late Proterozoic–Early Palaeozoic Alkhornet and Moefjellet units of the St Jonsfjorden Group and metacarbonates of Comfortlessbreen Group which are interpreted to record the main Caledonian metamorphic and deformational events (Morris 1988; Hjelle *et al.* 1999; Berg *et al.* 2003; Figs 2, 3). The Late Ordovician to Mid-Silurian Motalafjellet metacarbonates the lowest member of the Bullbreen Group (Kanat 1986; Hjelle *et al.* 1999) were also sampled to obtain a representative selection of metacarbonates from different structural settings in the study area. The palaeomagnetic properties of the sampled rock groups were then analysed to determine their possible contribution to palaeogeographic and tectonic reconstructions. To achieve the latter aim it will be necessary, therefore, to evaluate how far the geometry of the Caledonian structures of the study area was modified by the Late Cretaceous–Paleogene West Spitsbergen Fold Belt (WSFB) tectonics.

Earlier published palaeomagnetic data for Svalbard suggests that it was part of Baltica from Devonian time (Jeleńska and Lewandowski 1986; Nawrocki 1999; Michalski and Lewandowski 2004). More recently Michalski *et al.* (2012) have demonstrated that the Central and Eastern Terranes were part of Baltica from Silurian time. This latter work, in turn, draws attention to the question of the spatial relations between the Western Terrane of Svalbard and Baltica in Caledonian time, which is the focus of this study.

Geological setting

The structural evolution of the Caledonian basement exposed in the part of the Western Terrane of Svalbard (*e.g.* Harland 1997) under consideration here (Figs 1–3) is complicated by the Late Cretaceous–Palaeogene West Spitsbergen Fold Belt (WSFB) overprint. The WSFB, together with the Eureka Fold belts of North

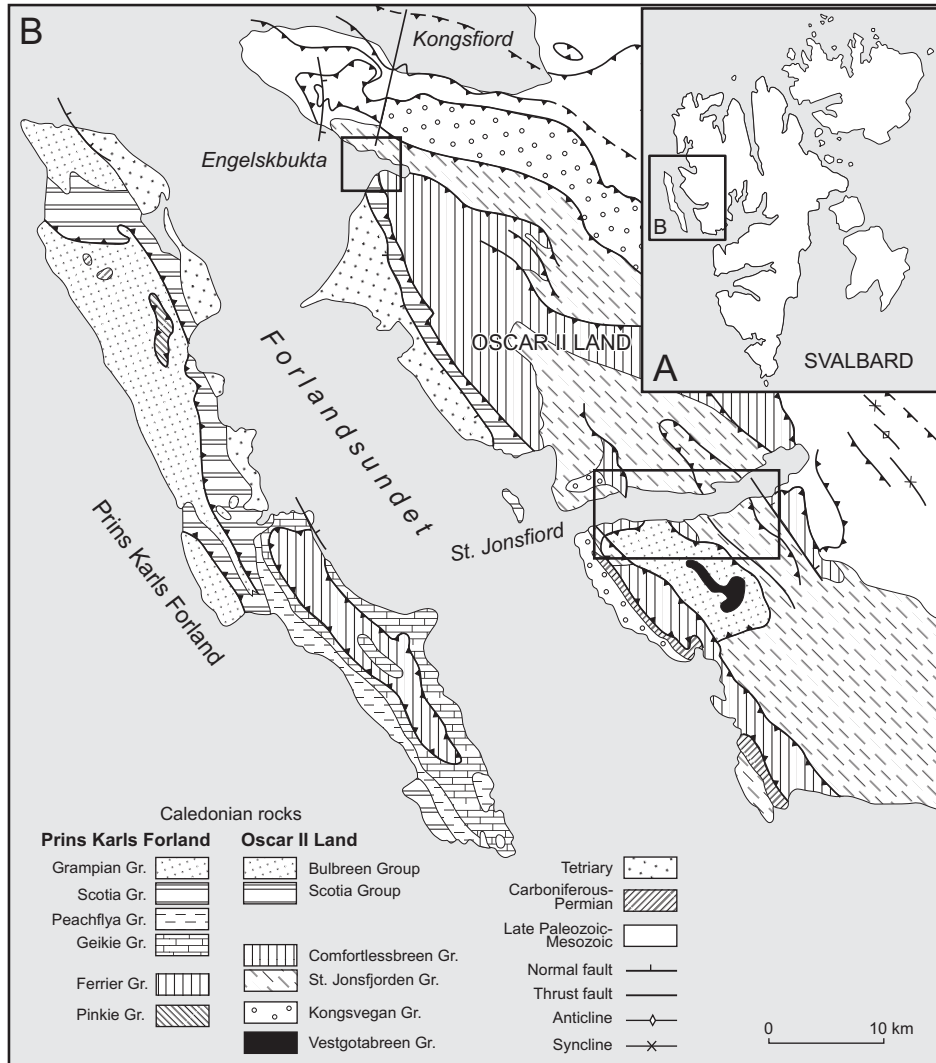


Fig. 1. **A.** Location of study area on the topographic map of Svalbard. **B.** Geological sketch of Prince Karls Forland and western part of Oscar II Land. Sampled areas (St. Jonsfjord and Engelsbukta) are marked by rectangles.

Greenland and Ellesmere Island, developed largely as a result of the *ca.* 200 km Greenland-Svalbard orthogonal convergence following the opening of the Labrador Sea-Baffin Bay before the opening of the North Atlantic-Eurasian Basins (Lyberis and Manby 1993; Manby and Lyberis 1996). The difficulties in distinguishing, in any detail, Caledonide structures from those generated by the WSFB arise, principally, from the lack of any thermal event accompanying the latter together with the lack of stratigraphic control and the different lithological responses to the post Caledonian deformation.

Some of the best exposed and most extensively studied segments of the target Western Terrane are to be found in the Central Oscar II Land (St Jonsfjorden) and the Brøggerhalvøya-Engelskbukta areas (*e.g.* Kanat 1986; Morris 1988; Lyberis and Manby 1993; Piepjohn *et al.* 2001; Tessensohn 2001).

St Jonsfjorden. — In the inner part of St Jonsfjorden and eastwards, Carboniferous to Triassic rocks are affected by a series of E to ENE verging thin-skinned fold and thrust nappes with ramp-flat geometries typical of foreland propagating fold and thrust belts (Welbon and Maher 1992; Lyberis and Manby 1993; Manby and Lyberis 1996; Bergh *et al.* 1997; Manby and Lyberis 2001). At the southern border of inner St Jonsfjorden (Vergardfjellet; Fig. 2) the Carboniferous rocks can be seen to be over-thrust by a sequence of west dipping thrust-fault bounded units with highly deformed and metamorphosed rocks of Caledonian origin, which dominate the structural architecture of the fjord region westward to the Forland-sundet trough. Mapping of the more westerly, Caledonide dominated nappes, suggests that they are rooted on shallow west dipping thrust faults with a more listric geometry characteristic of thick skinned fold and thrust belts (Fig. 2, cross-sections A–B, C–D). The sampled sites lie within two main thrust packages or units which have been mapped in detail by Kanat (1986) and Morris (1988). The lower thrust unit is considered to be of Late Proterozoic to Early Palaeozoic age while the upper thrust unit is of upper Ordovician to lower Silurian age.

Engelskbukta to Brøggerhalvøya. — The Engelskbukta to Brøggerhalvøya area represents the northernmost segment of the WSFB across which the thrust units change their transport direction. On the south side of Engelskbukta and for most of the WSFB to the south, folds and thrusts have an E or ENE. polarity. Across the northern part of Oscar II Land and toward Brøggerhalvøya transport swings around from an E-ENE to a NE direction (Fig. 3). The cause of this change in transport direction is controversial and further discussion of this is beyond the scope of this contribution (*cf.* Manby and Lyberis 1996; Bergh *et al.* 2000; Saalman and Theidig 2001, 2002).

Structurally, the Brøggerhalvøya area is interpreted to consist of a series of five nappes repeating the post-Devonian strata which are overthrust by four nappes (*cf.* Challinor 1967; Hinke 1989; Loske 1989; Piepjohn *et al.* 2001) consisting almost entirely of Proterozoic to Early Palaeozoic rocks that constitute Caledonian basement (Fig. 3).

Field work and methodology of laboratory experiments

Field work. — Palaeomagnetic samples were collected from twelve sites (Figs 2, 3). Each sample site was 20 to 40 meters in diameter and included several beds of metacarbonates. A total of 72 palaeomagnetic samples with the minimum dimension

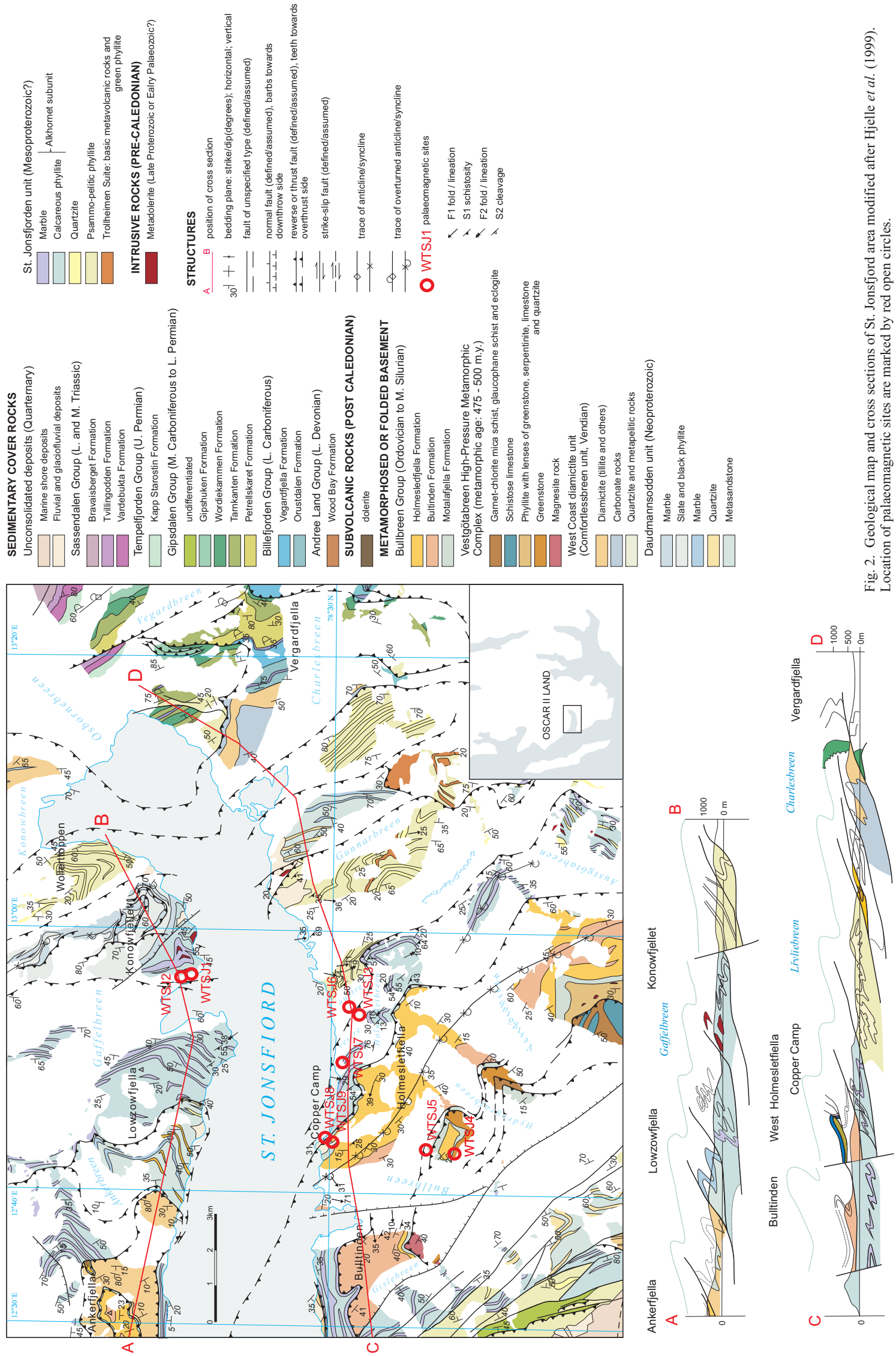


Fig. 2. Geological map and cross sections of St. Jonsfjord area modified after Hjelle *et al.* (1999). Location of palaeomagnetic sites are marked by red open circles.

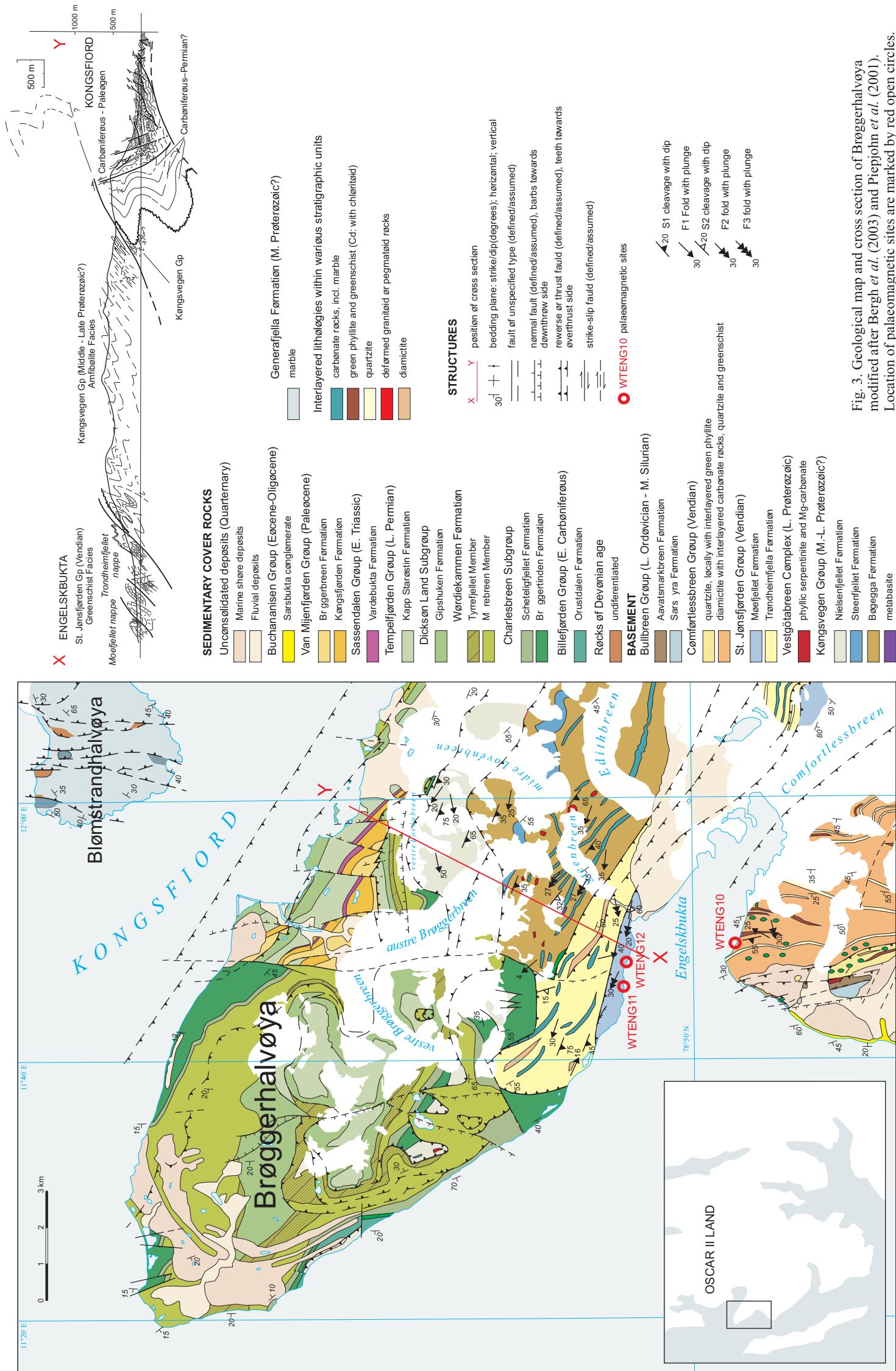


Fig. 3. Geological map and cross section of Brøggerhalvøya modified after Bergh *et al.* (2003) and Piepijnh *et al.* (2001). Location of palaeomagnetic sites are marked by red open circles.

15 cm² were independently oriented using a compass and retrieved from the fresh rock using a geological hammer (4–8 samples from each site). For each palaeomagnetic sampling site structural data was also gathered in the field and included measurements of the ductile, Caledonian, syn- to late metamorphic D1–D2 folds, foliations and reverse (thrust) faults. Measurements of the WSFB deformational structures, where distinguishable from those of Caledonian origin, were also gathered. Sampling, for later laboratory micro-structural investigation was also carried out to further aid the distinction of Caledonian and WSFB structural features.

Petrographical and mineralogical investigations. — Samples for petrographical examination of ferromagnetic phases were taken from the sample-set previously selected for rock-magnetic and palaeomagnetic investigations. Petrographic examination of textures and identification mineral species were carried out in transmitted and reflected light using NIKON ECLIPSE E600 POL, and NIKON ECLIPSE LV100 POL microscopes. Highly altered organic matter (graphite-like substances) was analyzed by epi-fluorescence microscopy using EX 380-420 filter. The large images of whole thin sections for textural examination were taken using MÄRZHÄUSER automatic XYZ stage controlled by NIS Elements AR 2.30 software.

The sub-microscopic ferromagnetic grains of Fe-, Ti-oxides, and Fe-S sulphides were examined using scanning electron microscope – SEM 120 FEI Nova NanSEM 200, equipped with a GEN121 ESIS XM4 EDS system. The resolution of this microscope is about 1 nm. The chemical compositions of the minerals were determined by electronprobe microanalysis (EPMA) using CAMECA SX100 apparatus, at the Inter-Institute Analytical Complex (Faculty of Geology, University of Warsaw). The microprobe was equipped with three WDS spectrometers. Acceleration voltage and current of the beam were 15 keV and 20 nA, respectively. Standard counting times were 20s on peak and 10s on both background positions. Natural and synthetic standards supplied by SPI and CAMECA were used during investigations.

Rock-magnetic experiments. — From each of 72 independently oriented samples up to 7 cylindrical cores (2.4 cm in diameter and 2.2 cm in length) were drilled for the Lowrie test (1990), anisotropy of magnetic susceptibility (AMS) and demagnetization procedures.

Detailed determination of $T_{ub\ max}$ (maximum unblocking temperature) and coercivity spectra of ferromagnetic phases was based on the three-component IRM (isothermal remanent magnetization) procedure described by Lowrie (1990).

In the first stage of the experiment 12 cylindrical cores representing all 12 sites were gradually magnetized along z-axis at room temperature up to 3T using MMPM-10 magnetometer. After each of the magnetization steps the IRM of the specimens was measured on the Superconducting Quantum Interface Device (SQUID, 2G Enterprise model 755, USA) with a residual internal field of below 3 nT and a noise level of about 5 μ A/m. The acquired IRM versus increasing applied

field was plotted on diagrams. This procedure gave the first approach to determining the coercivity of the specimens.

In the second stage cylindrical cores were magnetized along two following perpendicular axes in fields of 0.4T – along the y-axis and 0.12T – along the x-axis. The specimens were then subjected to a gradual stepwise thermal demagnetization in a field free magnetic furnace MMTD1 (Magnetic Measurements Thermal Demagnetizer, Great Britain). After each demagnetization step the magnetic signals of the specimens were measured on the SQUID. The experiment allowed an estimation of the coercivity fractions that dominate the specimens. Further, on three thermal demagnetization curves representing three low, intermediate and high coercivity perpendicular components magnetized along x, y and z axes respectively, it was possible to determinate maximum unblocking temperatures ($T_{ub\ max}$) of particular coercivity fractions.

Palaeomagnetic procedures. — Natural remanent magnetization (NRM) of all the cylindrical specimens prepared were measured on the SQUID. Maximum of 19 specimens per site with the highest values of NRM intensities were chosen for further demagnetization. Specimens for which the NRM intensity was below 0.05 mA/m were rejected for further analysis. The total number of 181 specimens were chosen for thermal demagnetization.

Before the demagnetization procedures the AMS values of all 181 specimens were measured on the Czech MFK1-FA, Agico susceptibility bridge. The AMS experiments were inconclusive and consequently discarded as they provided low magnetic susceptibility signals between 10^{-4} to 10^{-5} SI resulting in imprecisely defined principle AMS axes. The specimens were then heated in steps of 20–50° up to max. 680° ($T_{ub\ max}$ of hematite), and cooled to room temperature after each step in a zero magnetic field. After each demagnetization step the residual magnetic remanence was measured using the SQUID.

Simultaneously with the demagnetization process, the magnetic susceptibility (κ) of the specimens was monitored using a Czech low-field KLY-2 susceptibility bridge since changes of κ parameter can reflect the formation of new ferromagnetic minerals in the specimens during heating.

For visualization of palaeomagnetic data and calculation of NRM components, the characteristic remanent magnetizations (ChRM's) and the mean ChRM directions in particular sites, the Remasoft version 3.0 (Chadima and Hrouda, 2006) was used, which employs principal component analysis (PCA) after Kirschvink (1980) and Fisher (1953) statistics. The ChRM's were defined on the orthogonal Zijderveld diagrams as a direction of best fit line to a minimum of three points, with angular standard deviation (ASD) not exceeding 15° and, in 80% of the ChRM determinations not exceeding 10°. An exception was noted for site WTSJ6, where in particular specimens the WTSJ6L component, probably related to goethite, was calculated based on two temperature points of 50°C and 100°C. The ChRM directions were de-

terminated on the Zijderveld diagrams using “free line fit” and in the case of final stages of demagnetization an “anchored line fit” method (Butler 1992).

ChRM mean site directions obtained in this study were compared with the palaeomagnetic directions recalculated from the apparent polar wander path (APWP) of Baltica for Western Oscar II Land, Svalbard using GMAP 2012. The reference APWP of Baltica was derived from integral databases of GMAP 2012. For the purpose of recalculating the mean geographical location of the area investigated, the coordinates (78.5°N, 12°E) were used. Fold tests were not applied as a statistically significant mean direction was obtained for only one site. Spheristat (ver 3.2.1) software was used for the tectonic correction of the site means.

Structural setting of sample sites

Central Oscar II Land (OIL). — The palaeomagnetic sampling in the region of St. Jonsfjorden was focused on the dark grey limestones inter-folded with brown weathering dolomites of the Alkhornet sub-unit (lower package of Morris, 1988). On the southern shore of St. Jonsfjorden (Fig. 2, sites WTSJ 3 and 6–9) these limestones crop-out within a thrust unit that extends from near Copper Camp on the southern shore of the fjord across to Holmsletfjellebreen and onto Lovliefjella to the SE (Fig. 2, cross section A–B).

The floor thrust to the Alkhornet unit (Fig. 2, sites WTSJ 3 and 6–9) on the southern side of the fjord crops-out on the western flank of Lovliebreen where it dips a few degrees to the west before steepening to 25–30° as it crosses the lower slopes of Vestre Holmesletfellet westward of the shore line below sample site WTSJ7 (Fig. 2).

This thrust unit includes a metres-thick sequence of overlying orange weathering psammitic schists with millimetric to centimetric chlorite rich layers. To the west these rocks pass upwards into progressively thinner, brown weathering, psammitic beds with thicker dark slate interlayers. The roof thrust to this nappe can be observed on the slopes above Copper Camp (Fig. 2, sample sites, WTSJ 8 and 9) where limestones in footwall are overlain by a band of Bultinden-type conglomerates in the hanging wall. The conglomerate clasts are flattened and fragmented within the dominant foliation indicating a dextral, down dip (to the west), sense of shear (Fig. 4A), which is the opposite to that expected from the main thrust fault motion. The extent and direction of shearing may suggest that this thrust zone represents a west directed Caledonian thrust reactivated by the WSFB event. The limestones sampled at sites WTSJ 3 and 7 (Fig. 2) together with those on the nearby shore section are characterized by three phases of folding (Fig. 4B; see also Morris 1988). The first phase is manifest as a bedding parallel syn-metamorphic foliation associated with large, map scale, isoclinal folding of indeterminate vergence in the study area. The second phase folds are also tight to isoclinal while the third generation of folds comprises structures that are more often reverse kink to box type folds.

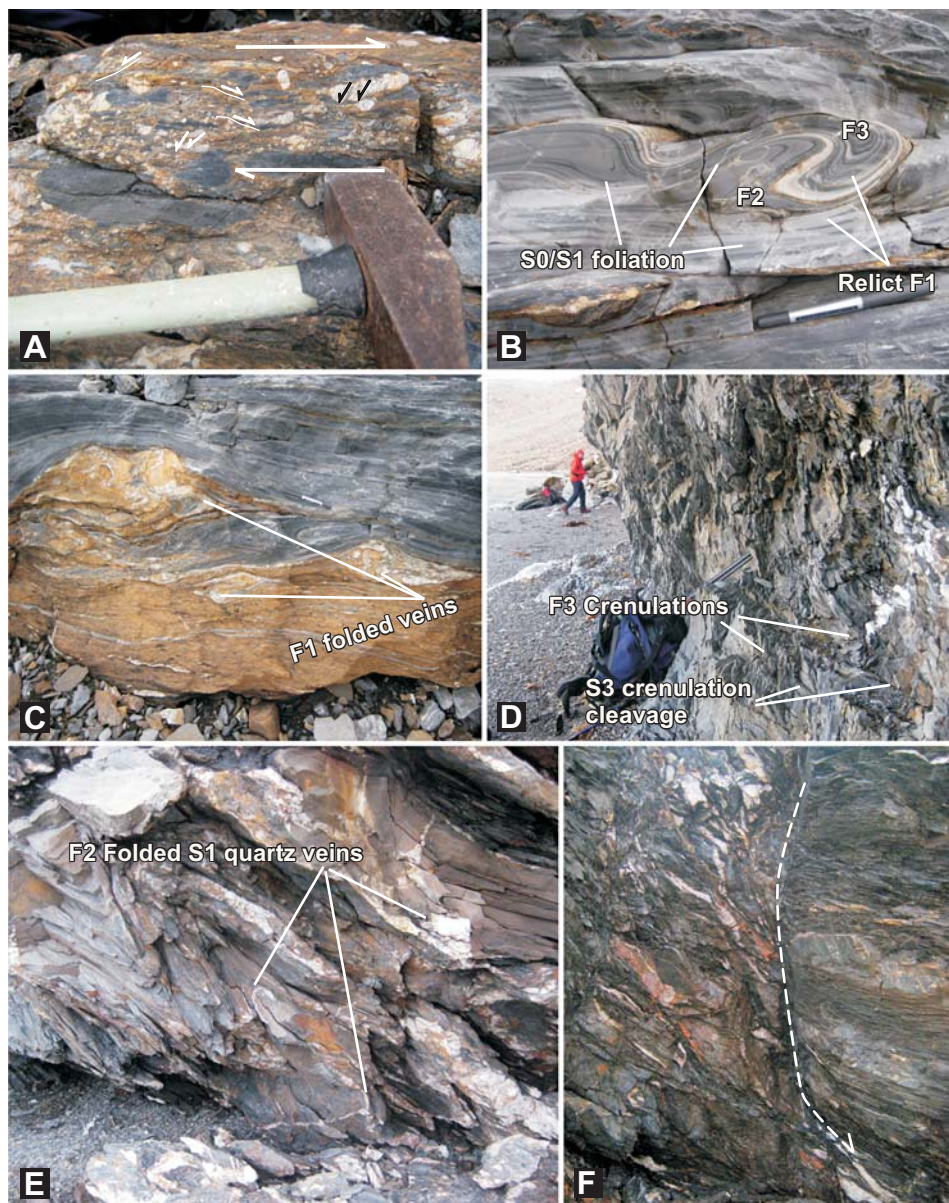


Fig. 4. Structural investigations of meta-carbonates from West Oscar II Land – part 1. **A.** Bultinden conglomerate on roof thrust zone of Alkhornet unit shows dextral shear sense. **B.** Grey Alkhornet marbles show 3 phases of ductile folding, S0/S1 is the bedding parallel metamorphic schistosity, some attenuated F1 fold closures are evident. Examples of small scale F2 and F3 folds are indicated. **C.** Small scale D2 ductile folded and boudinaged dolomitic marble band. Shows internal folding of calcite veins of D1 origin. **D.** Steep F2 limb of fold in Alkhornet Unit refolded by F3 fold with strain-slip cleavage dipping 45° west. **E.** Thin brown weathering psammites and black slates folded by F2/F3 ? folds. D1 quartz + dolomite veins are isoclinally folded in S1 foliation and refolded by east vergent F2/F3 folds. **F.** Example of one of the steep west dipping normal fault cutting the dark slate psammite sequence.

Extensive networks of calcite filled veins and tension gashes of early D1–F1 origin are found especially within the orange weathering dolomite layers. The more competent dolomite layers are boudinaged and extensively necked (Fig. 4C). The F1/S1 foliation, along with the boudins, is refolded by the F2 ductile folds which are accompanied by a more spaced west dipping axial planar S2 foliation. A steep limb of one of these F2 folds is refolded by the asymmetric east vergent centimetric scale F3 folds accompanied by spaced strain slip foliation (site WTSJ7, see Fig. 4D). Other F3 folds in this nappe are found on the ridge between the two branches of Holmesletfjelletbreen (Fig. 2, site WTSJ3). The proximity of these F3 folds to the floor thrust and coeval secondary thrusts suggests these are of the WSFB origin.

The fold sequence within the less competent dark slate rich overlying sequence of this lower package along the shore section toward Copper Camp is more complex. The large scale F1 fold closures were not observed but the main (S1) Caledonian schistosity and the early D1 tension gash strings are isoclinally re-folded by the highly ductile mesoscale F2 folds (Fig. 4E). The plunge directions of these later folds are not consistent and some degree of rotation by the later D3 (WSFB) thrust emplacement related deformation is evident. All of these structures are overprinted by a series of moderately west dipping small scale reverse faults. These faults are in turn cut by steep west dipping normal faults (Fig. 4F) with small slip amounts and they are often associated with shallow east dipping faults also with limited slip, which is suggestive of extensional collapse (Fig. 5A) following the WSFB nappe stacking. The steep west dipping normal faults are a prominent feature of the landscape particularly along the east-west ridges.

The Alkhornet unit limestones and dolomites were also sampled on the north shore of the fjord below Konowfjellet (Fig. 2, sites WTSJ 1 and 2). Here the sampled limestones and dolomites occupy a thrust slice where the roof thrust runs along the eastern margin of Gaffelbreen before crossing the fjord. A steep west dipping floor thrust, which is not illustrated on the cross-section but is shown on the map (Fig. 2), runs along the upper western slopes of Konowfjellet toward the fjord but is truncated by an east dipping normal fault before reaching the shoreline. The main Caledonian metamorphic S1 schistosity of the Alkhornet unit rocks in this slice is refolded by the east vergent F2 mesoscale folds (Fig. 5B) resembling those seen on the southern side of the fjord. The axial surface of the F2 folds at the sample sites changes, in an eastward direction, from a shallow to steep west dipping orientation. This F3 refolding of the limestones may be related to the WSFB deformation. Small scale crenulation folding with spaced axial planar pressure solution cleavages is seen to affect the steepened limestones to the east of the sample site (Fig. 5C).

Additional samples of the Motalafjellet formation limestones, which belong to the lower part of the Bullbreen Group (Kanat 1985; Bergh *et al.* 2003, 1:100,000 Geological Map) were taken from two sites (Fig. 2, WTSJ 4 and 5) on the nunatak SW of Holmesletfjellet. The nappe containing the Motalafjellet limestones also incorporates the exotic Vestgötabreen blueschist-eclogite grade group of rocks,

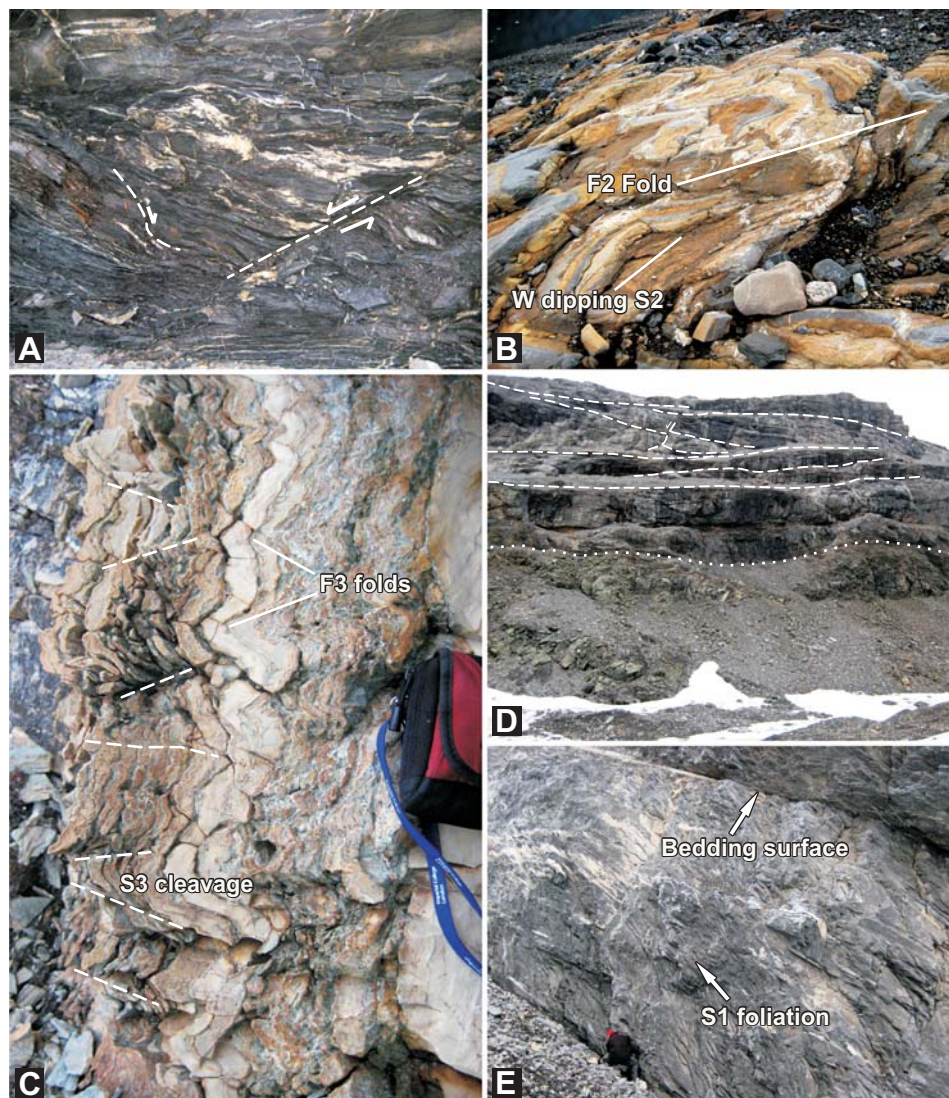


Fig. 5. Structural investigations of meta-carbonates from West Oscar II Land – part 2. **A.** Dark slates overlying rocks of Fig. 4E. Note the shallow conjugate east and west dipping normal faults indicative of extensional collapse. Similar structures are also seen in the slates along shore cliff below Ankerfjellet (Fig. 2). **B.** Mesoscale east vergent F2 folding of Alkhornet marbles, Konowfjellet shore. **C.** Small scale F3 folds with shallow west dipping strain slip cleavage in thin banded quartzites. **D.** Contact (indicated by dotted line) between Motallafjellet limestones and greenstones of the Vestgotabreen Complex. Note greenstones dip to right of view. The Motalafjellet Limestones (marbles) are cut by many wedge like thrusts (indicated by dashed lines). **E.** Thick bedded Motalafjellet marbles dip to right of view with steeper cleavage planes visible. Northwest Holmesletfjellet – Site WTSJ5.

which constitute the upper package of Morris (1988), are widely viewed to be part of a subduction zone complex (*cf.* Kanat 1985; Hirajima *et al.* 1988; Labrousse *et*

al. 2008). At sample site WTSJ4 (Fig. 2) the Motalafjellet limestones lie with an angular discordance above the southeasterly dipping greenstone member of this complex (Fig. 5D). The limestones are cut by numerous wedge-like shear surfaces which truncate the bedding surfaces at the contact with the greenstones implying a shallow southwest dipping thrust at the contact between the two units. At site WTSJ5 the sampled limestones are overlain by an overthrust sequence of the same limestones as seen at site WTST4 covered by a series of dark slates and psammites which are assigned to the Holmesletfjellet formation (Upper Bullbreen Group, see Kanat 1985; Bergh *et al.* 2003). The sampled limestones at site WTSJ5, on the lower slopes of the nunatac, are inverted and they are succeeded northward, along the arete leading to Holmesletfjellet itself, by the Holmesletfjellet Formation sandstones and slates and then the Bultinden conglomerate of the Upper Bullbreen Group. The Motalafjellet limestones passing down into the Bullbreen group rocks along this ridge occupy the inverted limb of a large scale NW-SE trending, SE plunging, synclinal fold overturned to the NE (Fig. 2, cross section A–B).

This overturned syncline lies above the roof thrust to the Alkhornet thrust unit described above. The Bullbreen Group, including the Motalafjellet limestones (marbles) appear to be weakly metamorphosed and the axial planar fabric to the overturned fold on the arete is expressed as a pressure solution cleavage (Fig. 6C). The marble has a porphyroblastic texture with irregular porphyroblasts showing strain induced twinning while the matrix grains are more equant indicative of recovery recrystallization. This fold structure although attributed to the WSFB by many authors (Kanat 1986; Morris 1988; Manby and Lyberis 2001) may be, in the light of the foregoing observations, of Late Caledonian origin. The northeastern right-way-up limb of the syncline is kink folded and truncated by the a floor thrust to this nappe. The syncline has the same vergence as the mesoscale F2 folds in the underlying Alkhornet unit nappe described earlier. The Motalafjellet limestones of the lower Bullbreen Group which cap the blueschist-eclogite rocks are viewed as a Late Caledonian sequence deformed during the syn-collisional exhumation of the entire complex (Labrousse *et al.* 2008) supporting an origin of the above syncline in this time interval.

Based on the cross sections presented in Fig. 2, it seems likely that the WSFB related folds in post-Caledonian rocks formed as fault-bend or fault-propagation folds related to the ramp-flat changes or the ductile beads ahead of thrust tips, respectively. A possible position of the folded cover unconformity is projected westward along the line of section with the suggestion that these hypothetical folds are also fault propagation in origin. Restoration of these structures to the pre-WSFB deformation situation would result in a shallowing of the westerly dip of thrust sheets as the nappes are restored to a position they may have occupied prior to ascending any listric or ramp-like structures. With the exception of the overturned fold affecting the Bullbreen Group, described above, the underlying nappes show only large scale flexuring of the D1–D2 structures in addition to the small scale F3 folds developed near the main thrust faults mentioned above.

Brøggerhalvøya-Engelskbuta. — In this area the target rocks were the dark grey silty meta-limestones with thin black slates that lay a few meters above the floor thrust to the Moefjellet nappe (sites WTENG 11 and 12) on the north shore of Engelskbuta (Fig. 3).

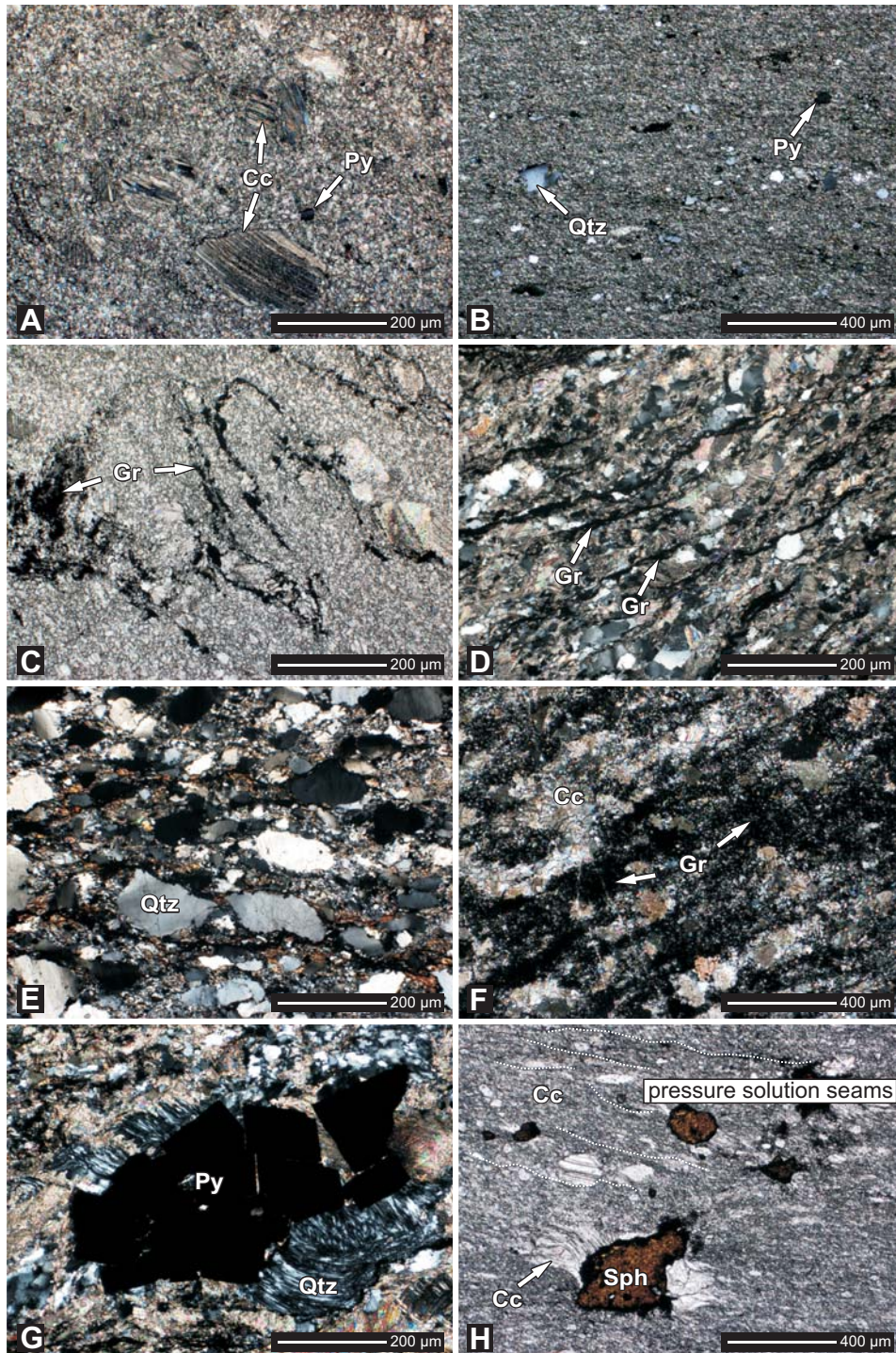
At site WTENG 11 the main Caledonian D1–F1–S1 schistosity is bedding parallel with dips and strikes ranging from 124/46SW to 144/52SW. F2 folds, which re-fold the S1 schistosity, plunge 143/22 with an axial planar cleavage oriented 136/67SW and numerous small scale reverse faults striking 122/52SW disrupt these folds. Accompanying these small thrust faults are series of steep NW dipping dextral normal faults. At site WTENG12 the bedding parallel S1 schistosity is steep, oriented 150/70W and it is refolded by 167/0 trending F2 micro-crenulation folds with a 006/30E (transverse) oriented axial planar foliation. These structures are again cut by shallow NE dipping reverse faults accompanied by 120/55SW oriented dextral normal faults.

A feature of the north shore of Engelskbukta is the presence of small scale thrust faults generating imbrication of the component rock sequences. Many of these small scale thrust faults are observed to have curved trajectories which effectively rotate the affected F2 folds to the SW about NW/SE axes. The floor thrust related faults at the base of the Moefjellet nappe/roof of the Trondheimfjellet nappe, exposed at a short distance to the NW of the site WTENG11, on the lower slopes of Bjorvigfjellet, are oriented 100/70S.

The Caledonian rocks of the Trondheimfjella Nappe which are of chlorite to biotite grade are thrust in the NE direction over the Bogegga Nappe which contains higher, amphibolite, grade garnet-biotite schists, coarsely crystalline white marbles, rare migmatites pods and garnet amphibolites (see also Hinke 1989; Loske 1989).

On the southern shore of Engelskbukta at site WTENG10 the sampled rocks are dark grey thin bedded limestones with black slaty interlayers which on the map of Berg *et al.* (2003) are assigned to the Comfortlessbreen, diamicitite succession. The general orientation of the main bedding parallels here the Caledonian S1 foliation and varies from 006/64W to 168/41W.

Fig. 6. Photomicrographs of metacarbonate rocks (under cross polarized light). **A.** Granoblastic marble from St. Jonsfjord where larger grains show strain induced twinning. **B.** Granoblastic marble sample with quartz and opaque minerals defining S1 foliation. St. Jonsfjorden. **C.** Micro-folds/stylolites within the granoblastic marble, enriched in organic matter, sample from St. Jonsfjorden. Evidence of S2 pressure solution seams bottom left of image. **D.** Foliated, calcite-bearing siliciclastic rocks with a large proportion of quartz; rich in organic matter (Engelskbukta). **E.** Foliated, siliciclastic rocks from St. Jonsfjorden traversed by irregular pressure solution seams. **F.** Foliated, granoblastic marble sample, enriched in organic matter (Engelskbukta). Graphite seams define foliation. **G.** Pyrite grain with well developed pressure fringe containing rotated quartz fibers (Engelskbukta). **H.** Sphalerite grains within granoblastic marble of St. Jonsfjord and slightly rotated (dextral) calcite pressure fringes developed during late stages of recrystallization of marble. S1 is defined by elongate carbonate grains. Some weakly developed pressure solution seams top right of image. Abbreviations: Cc – calcite, Gr – graphite-like substance, Qtz – quartz, Py – pyrite, Sph – sphalerite. →



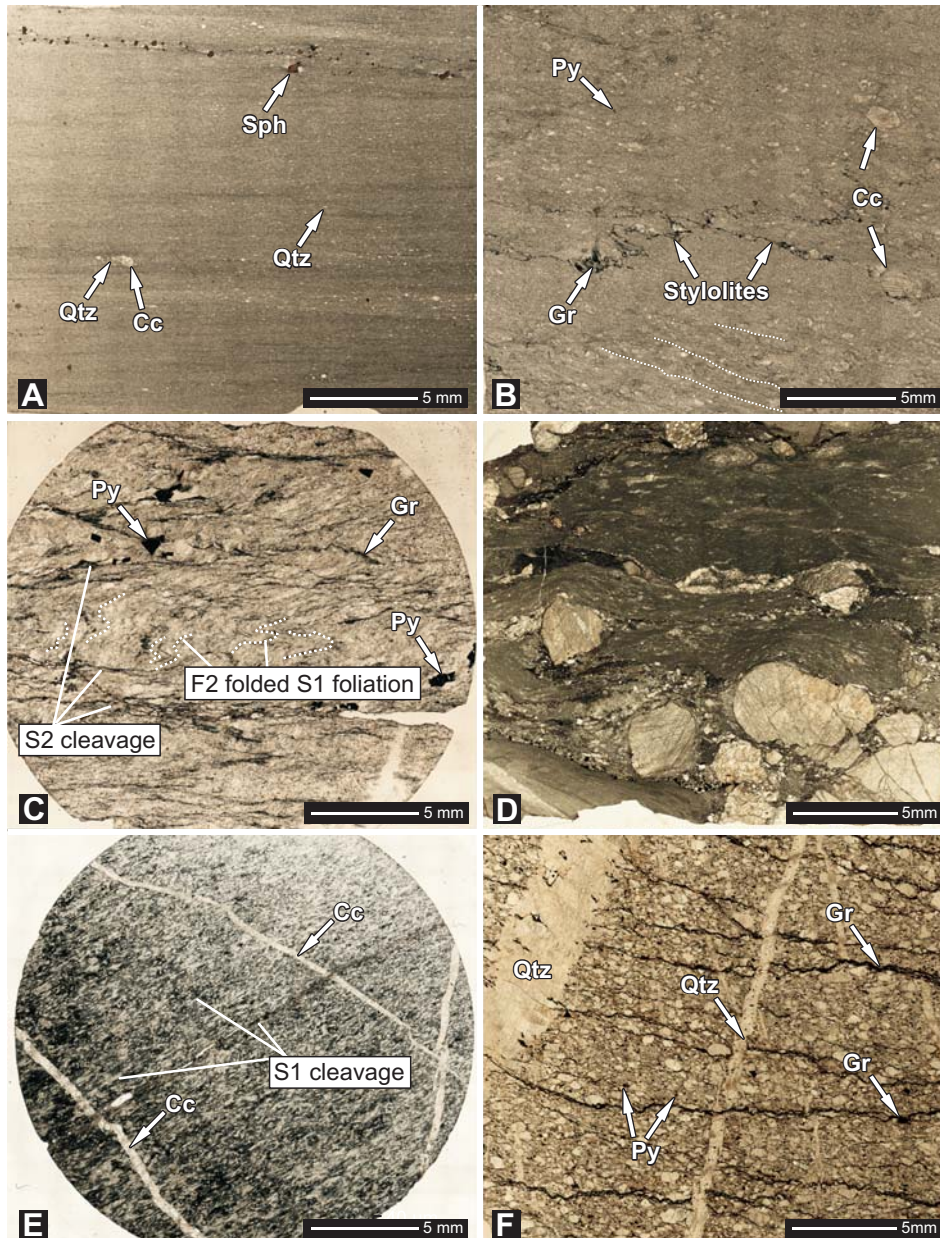
The meta-limestones are characterized by extensive calcite vein material generated early in the D1 Caledonian deformation in the form of large tension gashes accompanying structures which have been flattened, boudinaged and rotated into parallelism with the S1 schistosity. The later F2 folding is often associated with further calcite veining which is variously truncated by the S2 cleavage surfaces. The orientation of the F2 folds along the exposed section sampled is variable ranging from over turned, steeply plunging to flat-lying NW-SE trending structures. Steep east dipping, N-S striking reverse faults are common. In the more shallowly dipping slaty parts of the section sampled an extensional kink-like folding is found with a down-to-the-west sense of slip.

It is clear that the Caledonian rocks in this area were actively involved not only in the WSFB deformation (*e.g.* Challinor 1967; Manby and Lyberis 1996; Piepjohn *et al.* 2001; Saalman and Theidig 2001, 2002) but also record significant extensional faulting associated with the formation of the Forlandsundet Trough and extension related to the opening of the Eurasian Basin (see Manby and Lyberis 1996).

Petrography of investigated metacarbonates

Petrographic examination of the sampled metamorphosed carbonates from Western Oscar II Land has revealed that they are texturally varied marbles (Figs 6A–C, H, 7A–C) interbedded with intercalations of meta-pelite, meta-psammite, and meta-conglomerates (Figs 6E, 7F). The concentration of quartz and aluminosilicates within the carbonate-rich layers varies from very small amounts in the marbles of St. Jonsfjorden area to in excess of 50 vol. % in the Engelskbukta marbles (Fig. 6D, F). The textures of the marbles vary, from fine-grained granoblastic

Fig. 7. Example of recrystallization textures of marbles from St. Jonsfjord and Engelskbukta areas (Western Terrain, Svalbard). All microphotographs were taken under transmitted light, one nicol. **A.** Fine-grained marble with weakly expressed S1 foliation. Some compositional variation is apparent (S0) parallel to S1. The foliation planes are defined by the preferred orientation of fine lenticular blasts of the quartz and/or calcite. A fine zone of large sphalerite grains is visible in upper part of the image. The sphalerite crystallized before final recrystallization of the marble as indicated by well developed pressure fringes (see arrowed sphalerite grain). Site WTSJ7. **B.** Marble with well developed porphyroblastic texture. Relics of older foliation planes are defined in lower part of the image. The black lines at the central part of the image are concentration of graphitic-like substance concentrated along a (pre-schistosity, S1?) stylolitic surface. Site WTSJ5. **C.** Marble showing flattened carbonate blasts defining the S1 foliation planes crenulated by F2 microfolds (dotted lines). The accompanying S2 foliation is defined by the dark to black, widely spaced, graphite rich seams. Site WTENG10. **D.** Strongly sheared (dextral) to mylonitized, carbonate metaconglomerate. Site WTSJ9. **E.** Uniformly distributed highly altered organic matter (organic-like substance; black in colour) within a quartz-bearing metacarbonate, the flattened fine quartz grains define the S1 foliation (Caledonian). Note that the high angled cross-cutting calcite veins are slightly disrupted as they intersect the S1 foliation suggested they developed during a very late stage of the S1 development. Site →



WTSJ1. F. Psammitic band within the examined marbles. The abundant quartz grains show dimensional preferred orientation and define the S1 (?) foliation. Anastomosing, dark graphitic (pressure solution) S2 (?) seams cut by quartz veins. The wider NNE-SSW vein to the right includes thin discontinuous dark seams – pre-S2. The narrow NNE-SSW vein to the left is intersected by discontinuous NNW-SSE veins which appear to be Riedel shears. Together these veins are consistent with a principal compression direction parallel the two NNE-SSW veins and perpendicular to the S2 pressure solution seams. Site WTSJ6. Abbreviations: Cc – calcite, Gr – graphite-like substance, Qtz – quartz, Py – pyrite, Sph – sphalerite.

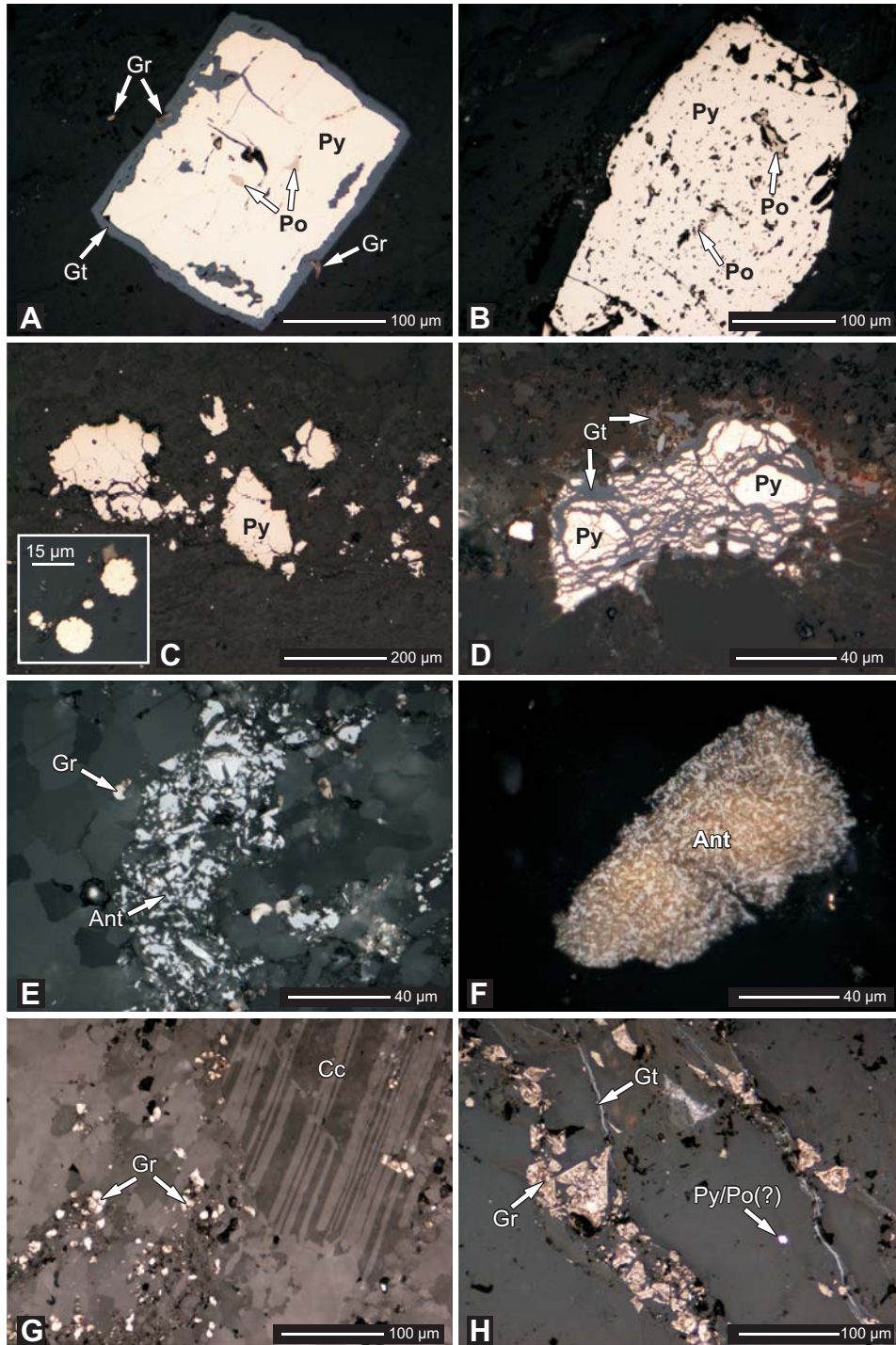
(homoblastic) to fine-medium-grained porphyroblastic. Micro-structurally some of the metacarbonates exhibit a penetrative syn-metamorphic S1/S2 (?) foliation defined by grains with a dimensionally preferred orientation. This fabric is often seen to be overprinted by a more spaced pressure solution cleavage which is found in some samples to be axial planar to small scale crenulation folds. Other samples preserve, in addition, stylolitic surfaces overprinting the earlier S0/S1 foliation. The foliation planes, folds and stylolites are defined by microscopically visible thin zones rich in thermally degraded organic matter (Figs 6C–D, 7B–C, F), for which the reflectivity exceeds 3%. These aggregates have optical features (anisotropy, reflectance) typical of graphite-like substance (see Fig. 8G–H).

The investigated metamorphosed carbonates can be divided into four distinct types:

Type I: Pure marbles, containing almost 100% carbonate minerals (calcite +/-dolomite) characterized by equigranular, granoblastic textures (Fig. 6A–B). This type of marble is typical of samples collected from the St. Jonsfjorden area. Locally, millimetric micro-folds, enhanced by the presence of organic matter are visible (Fig. 7C). In some locations these marbles contain small amounts of recrystallized, elongate, lens-like quartz grains, Na- and K-feldspars, chlorite, and muscovite flakes that additionally define the S1 foliation planes. The marbles and metamorphosed siliciclastic interlayers are commonly cut by thin calcite and quartz veins (Fig. 7E–F).

Type II: Metamorphosed calcite-bearing siliciclastic rocks (Fig. 6D, F), which contain up to 50% quartz, feldspar, muscovite, chlorite, and other fine-grained aluminosilicates. This type of rock was common within samples collected from the Engelsbukta area. These rocks are also rich in organic matter that occur as primary dispersed aggregates within carbonates (Fig. 6F) and secondary concentrations along foliation planes, micro-faults and 2 stylolites (Figs 6C–D, 7B–C). The lens-like quartz grains document intensive metamorphic recrystallization of the rocks. Some larger grains of quartz, pyrite and sphalerite grains are rimmed by deformed, quartz and/or calcite pressure fringes (generated by pressure-temperature enhanced diffusion) that clearly show rotation of these grains probably during the Late Caledonian deformation (Fig. 6G–H).

Fig. 8. Mineralogy and textural relationships within ferromagnetic associations. All microphotographs were taken under reflected light, one nicol. **A.** Euhedral pyrite grain with pyrrhotite intergrowths. The pyrite is replaced by late goethite/lepidocrocite. The host marble contains minute blebs of graphite-like substance. Site WTSJ6. **B.** Numerous pyrrhotite intergrowths within pyrite. Site WTENG10. **C.** Metamorphosed pyrite aggregates reflecting their granoblastic equigranular texture. Red arrow indicates pyrite grains. The inset shows example of recrystallized framboidal pyrite aggregates, that are very common in all examined metacarbonates. Site WTSJ9. **D.** Pyrite aggregate, located along foliation plane, replaced by late Fe-hydroxides (goethite). Site WTSJ9. **E.** Fine-grained anatase grains associated with graphite-like substance. Site WTSJ5. **F.** Anatase (TiO₂ oxide) pseudomorph after detrital ilmenite. Site WTSJ6. **G.** Rounded, graphite-like aggregates distributed within calcite porphyroblast and within fine-grained granoblastic matrix. Site WTSJ5. **H.** Accumulation of graphite-like substance along foliation plane. Site WTSJ6. Abbreviations: Ant – anatase, Cc – calcite, Gr – graphite-like substance, Gt – goethite, Qtz – quartz, Po – pyrrhotite, Py – pyrite.



Type III: Siliciclastic rocks composed mainly of deformed quartz, muscovite, K- and Na-feldspars, chlorite, fine grained clay minerals, and subordinate amount of carbonates (Figs 6E, 7F). These rocks shows directional textures that originated during metamorphism as evidenced by deformed quartz grains, and foliation planes defined by the presence of aligned metamorphic phyllosilicates (muscovite, chlorite) and seams of graphite-like substance.

Type IV: Conglomerates. The clasts in the conglomerates often consist of metamorphosed and highly strained carbonates, carbonate-silicate rocks, siltstones, and sandstones (Fig. 7D). The matrix of the examined conglomerates consists of mixture of fine-grained carbonates and phyllosilicates. The conglomerates are also rich in thermally degraded organic matter.

All of the investigated samples commonly contain variable amounts of pyrite. The size of pyrite grains varies from sub-microscopic to 0.5 cm in diameter. The enhanced pyrite accumulations were observed in samples rich in organic matter. Small pyrite aggregates resemble recrystallized primary framboidal pyrites formed during a diagenetic stage of evolution of the rocks, while the largest example grew, unequivocally, during metamorphism (Fig. 6G).

All investigated samples were cut by thin calcite and/or quartz veins (Fig. 7E–F) that indicate high activity of H₂O–CO₂ rich fluids. The fluids are responsible for mobilization of the Cu, Pb, Zn, Ni, Fe, As, and other metals from siliciclastic intercalations during metamorphism, which then crystallized as metamorphic sulphides within marbles. Such fluids also significantly enhanced the oxygen fugacity that controlled the stability of Fe–Ti- and Fe-oxides (Frost 1991a; 1991b; Haggerty 1976; 1991). The petrographic and rock-magnetic investigations indicate that hematite/maghemite associations are subordinate components of all of the examined rocks. The presence of these associations is the result of dissolution of magnetite during the rock-fluid interactions and breakdown of the Ti-magnetite and ilmenite into TiO₂ oxides (Fig. 8C). These processes are well documented petrographically by the occurrence of anatase/brookite (leucosene) pseudomorphs after ilmenite (Fig. 8F). This general trend may be locally reversed by enhanced concentrations of organic matter (OM) that also were thermally degraded and recrystallized during metamorphism (Figs 6C–D, F, 7B–C, F, 8G–H). The sedimentary OM, manifest as a graphite-like substance, has thus locally preserved the stability field for pyrrhotite and hematite/maghemite. The high activity of sulphur during metamorphism, that was controlled by numerous aggregates of framboidal pyrites and partly by OM (Fig. 8C), probably led to the replacement of primary magnetite and pyrrhotite by pyrite. The final effect is the almost complete dissolution/breakdown of Fe- and Fe–Ti-oxides and the local preservation of pyrrhotite, mainly within largest pyrite grains and or calcite blasts (Fig. 8A–B, H). All of the pyrrhotite aggregates are unequivocally of metamorphic origin and must have been, therefore, generated during the Caledonian greenschist facies metamorphism.

Identification of ferromagnetic minerals

Optical and electron microscopy investigations. — The ferromagnetic minerals recognized during the petrological investigations are represented mainly by pyrrhotite and goethite. Hematite/maghemite (?) occurs in small amounts, and was only determined during the SEM and rock-magnetic investigations. Ferromagnetic minerals were recognized within marbles, and within the intercalated psammites and pelites, where they are also associated with pyrite, sphalerite, galena chalcopyrite, TiO₂-oxides (brookite and/or anatase), titanite, and a very common graphite-like substance (Fig. 8E, G–H).

Pyrrhotite, according to rock-magnetic experiments, is the main ferromagnetic carrier in the investigated metacarbonates. This mineral commonly occurs as the inclusions within pyrite (Fig. 8A–B). The minute oval grains of pyrrhotite were also recognized within calcite blasts. Pyrite forms separate grains from submicroscopic minute crystals to large grains up to 0.5 cm in diameter as well as aggregates of different sizes partly recrystallized along foliation plane (Fig. 8C). A common feature of the marbles was the occurrence of aggregates of framboidal pyrite, that were recrystallized and deformed (see inset in Fig. 8C). The recrystallization processes are documented by the equigranular texture of the pyrite aggregates and the occurrence of calcite-quartz pressure-fringes (Fig. 6G). Pyrite very often forms paragenetic associations with sphalerite and chalcopyrite. The larger pyrite and sphalerite grains, that acted as rigid bodies during metamorphic recrystallization (Fig. 6G–H), clearly show that they originated during the Caledonian metamorphism. Observations of the textures and spatial relations between identified sulphides leave no doubt that pyrite-pyrrhotite-chalcopyrite-sphalerite belong to the same metamorphic association.

Small amounts of fine maghemite/hematite were recognized within the marbles containing increased concentration of organic matter. This may be explained by a lowering of the oxygen fugacity during metamorphism. The Fe-Ti oxides, that are a common component of metasedimentary rocks, are represented in the investigated metacarbonates mainly by low temperature Ti-oxides, *e.g.* anatase and/or brookite (Fig. 8E). All detrital ilmenite and magnetite grains within the organic matter rich limestones were first re-crystallized during diagenesis and early stages of metamorphism and later converted to anatase/brookite or magnetite/maghemite, respectively. This is evidenced by numerous, small dispersed grains of Ti-oxides within the marbles (Fig. 8E) and leucoxene pseudomorphs after detrital ilmenite grains (Fig. 8F).

Rock-magnetic experiments. — Optical and microprobe EDS observations were followed by rock – magnetic experiments. In the majority of sampling sites the IRM acquisition curves (Fig. 9) show the dominance of a soft-medium coercivity fraction saturated in 0.1–0.4 T. The samples from sites WTSJ6 and WTSJ7 do not saturate in the maximum applied field of 3 T, revealing existence of high coercivity minerals.

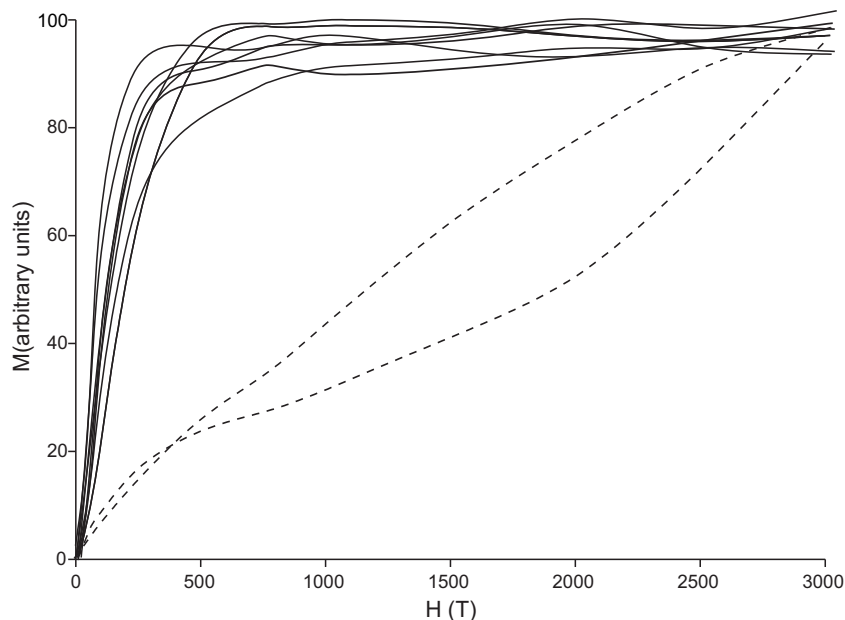


Fig. 9. Examples of IRM (isothermal remanent magnetisation) analysis of metacarbonates from Western Oscar II Land. Dashed lines represent specimens from sites WTSJ6 and WTSJ7 which do not saturate in max. applied field – 3T.

In ten out of twelve investigated sites, thermal demagnetization curves of the three component IRM acquisition experiments (Lowrie 1990) reveal the dominance of soft and medium coercivity fractions saturated up to 0.12 T and between 0.12–0.4 T respectively, with distinct temperatures around 250–375°C, 425–450°C and 500–575°C (Fig. 10A–B, E–F). The range of temperatures 250–375°C can be related to the demagnetization of pyrrhotite ($T_{ub\ max} \sim 325^\circ\text{C}$; Dekkers 1989), which was recognized in the examined thin sections (Figs 6A–B, G, 8A–D). The 425–450°C (Fig. 10E) range of temperatures may be an indication of maghemite or Ti-rich magnetite. The existence of the latter phase is less probable since microscopic observations indicate the extensive breakdown of ilmenite into TiO_2 phases – anatase, brookite (Fig. 8E–F). The values of 500–575°C are close to the $T_{ub\ max}$ of moderate to low Ti magnetite (Dunlop and Özdemir 1997).

Hard coercivity fractions saturated above 0.4T in the field up to 3T are dominant in only two sites – WTSJ6 and WTSJ7 (Fig. 10C–D). In these sites the high coercivity curves record additionally distinct temperatures 100°C and 680°C which are close to the $T_{ub\ max}$ of goethite and hematite (Dunlop and Özdemir 1997).

Mineral chemistry of silicates and sulphides

Silicates and sulphides constitute a subordinate component of the examined metacarbonates. The mineralogy of silicates is dominated by dioctahedral phyllo-

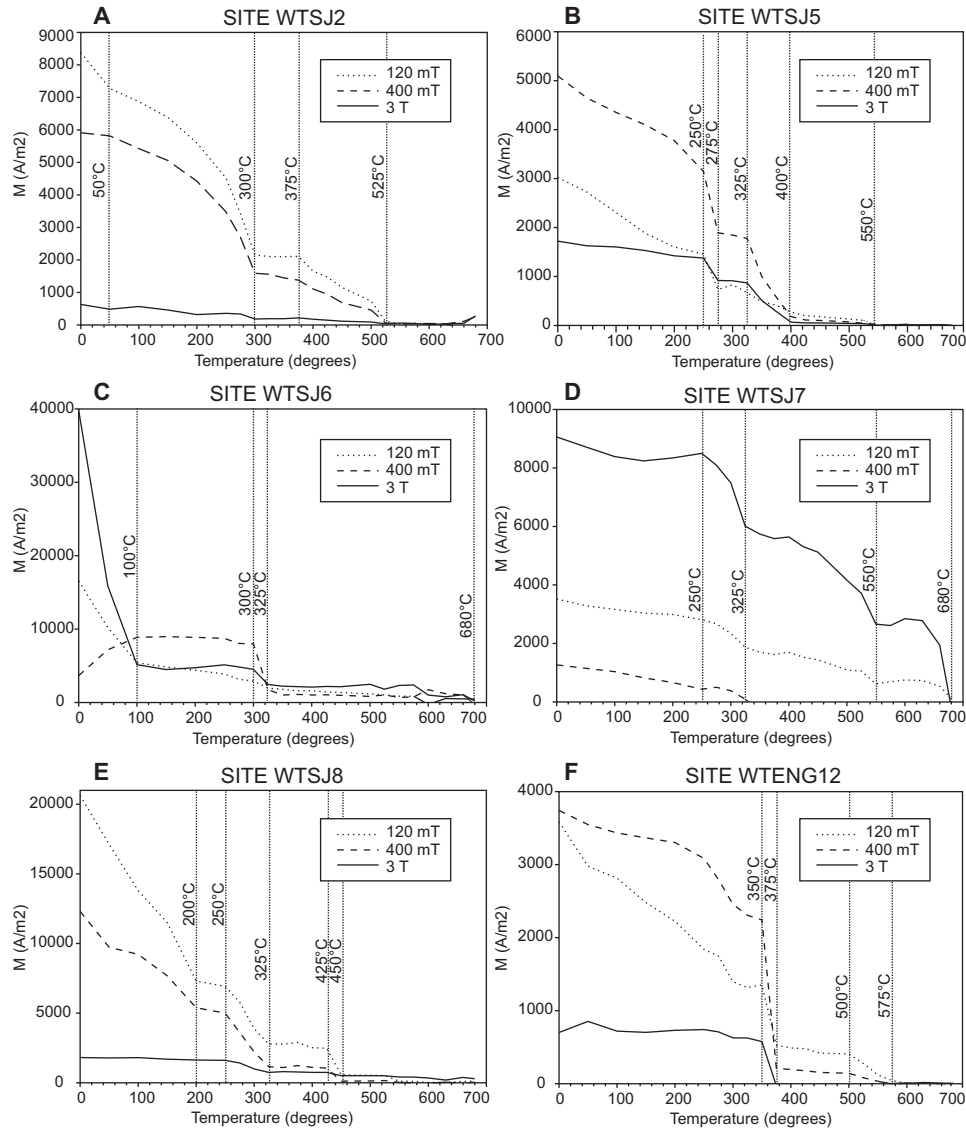


Fig. 10. Examples of three-component IRM acquisition curves (Lowrie, 1990) analysis of metacarbonates of Western Oscar II Land. Changes of slope of the demagnetization curves are marked by dotted lines and the temperatures of these points are given. Particular curves show demagnetization of different coercivity fractions existing in the samples: solid lines – ferromagnetic particles saturated between 400 mT and 3000 mT; dashed lines – those saturated between 120 mT and 400 mT; dotted lines – those saturated below 120 mT. M – normalized magnetization of the samples.

silicates (muscovite), and subordinate fine-grained chlorite. Other common silicates are quartz, and feldspar. The sulphide association consists of pyrite, pyrrhotite, sphalerite, galena, chalcopyrite. In some sulphide aggregates small barite intergrowths were identified.

Feldspars are chemically homogenous (Ab *ca.* 99 %), in contrast to the muscovites, that vary in texture and chemical composition (Table 1A). Representative analyses of the white micas are shown in Table 1A. Si fills the range from 6.03 to 6.93 apfu, while Fe/(Fe+Mg) ratio varying from 0.13 to 0.67. The metamorphic mineral assemblage in all examined samples is formed by Cal + Dol + Qtz \pm Ms (Ph) that clearly indicate conditions typical of greenschist facies metamorphism. Based on mineralogy and chemistry of silicates the temperature of metamorphic recrystallization did not exceed 400°C (for comparison see Lupták *et al.* 2003).

The chemical concentration of Fe and S in pyrrhotite ranges from 58.06 wt% to 59.96 wt%, and from 35.32 wt% to 40.01 wt%, respectively (Table 1B). The Ni contents in pyrrhotite is low and commonly ranges from 0.47 wt% to 0.92 wt%. In some pyrrhotite-like minerals the concentration of Ni reaches up to 29.15 wt% while Fe is close to 33.9 wt%, suggesting the presence of pentlandite (Table 1C). The Fe/S atomic ratio in most of the examined pyrrhotite grains varied from 0.84 to 0.88 (Table 1B). This ratio is typical of monoclinic pyrrhotite with 4C superstructure (Fe₇S₈), for which the Fe/S atomic ratio commonly varies from 0.84–0.88 (Powell *et al.* 2004; Becker *et al.* 2010). The highest ratios ranging from 0.88 to 0.91 and from 0.91 to 0.93 characterize the hexagonal pyrrhotites with 5C (Fe₉S₁₀) and 6C superstructures (Fe₁₁S₁₂), respectively (Becker *et al.* 2010). The latter two polytypes did not reveal any ferromagnetic properties (Tokonami *et al.* 1972; Morimoto *et al.* 1975; Kontny *et al.* 2000; Powell *et al.* 2004).

The chemical composition of pyrite is close to stoichiometric, Fe and S content ranges from 46.22 wt% to 47.15 wt%, and from 52.94 wt% to 53.71, respectively (Table 1). The concentration of Ni suggests the occurrence of two groups of pyrite; a group of Ni-bearing pyrites, where the concentrations of Ni reach 0.5 wt%, and another group where Ni is constantly below detection limits. This suggests that the latter group may represent recrystallized diagenetic pyrite (Ni-low), while the former Ni-bearing group could represent a truly metamorphic phase which grew at the time when Ni and Fe were mobilized from silici-clastic intercalations. The paragenetic association of pyrite with galena, sphalerite, chalcopyrite and barite would support such an interpretation. During the later stages of evolution of the marbles, the pyrite, pyrrhotite, and chalcopyrite were commonly replaced by goethite (Fig. 8A, D).

Sphalerite recognized during petrographic investigations is unequivocally metamorphic in origin (Fig. 6H). All of the analyzed sphalerite grains are characterized by low Fe content which varies from 1.41 wt% to 2.44 wt%. The X_{FeS} content is low and reach up to 4.25% (Table 1D). Sphalerite associated with pyrite-pyrrhotite is used as a single geobarometer. Numerous calibrations are available; most commonly used geobarometers are based on experimental results of Scott (1973), Lusk and Ford (1978) and Martín and Gil (2005). An application of these geobarometers to low X_{FeS}, determined in the examined sphalerites (see Table 1D), give pressures that exceed 10 kbar. It has been suggested, however, that

Table 1
 Representative chemical composition of silicates, pyrrhotite, pyrite, and sphalerite occurred in examined metacarbonates.
 Abbreviations: b.d.l – concentrations below detection limits.

A. Selected chemical analyses of dioctahedral phyllosilicates (x1–x8), chlorite (x9), and feldspars (x10–x12).

Sample No.	WT-4303 x1	WT-4303 x2	WT-4303 x3	WT-5801 x4	WT-5801 x5	WT-5801 x6	Ang-t2 x7	Ang-t2 x8	WT-4303 x9	AngsT-2 x10	AngsT-2 x11	AngsT-2 x12
SiO ₂	53.02	43.21	45.50	44.84	49.45	50.46	51.03	51.39	30.76	68.91	68.83	68.48
TiO ₂	0.14	0.20	0.13	2.86	0.10	0.21	0.31	0.29	b.d.l.			
Al ₂ O ₃	26.47	25.64	26.02	33.81	37.32	32.36	30.47	29.34	19.72	19.71	19.69	19.60
Cr ₂ O ₃	b.d.l.	0.12	0.22	b.d.l.	b.d.l.	b.d.l.	b.d.l.	b.d.l.	0.15			
FeO	3.83	3.72	3.00	1.93	0.78	3.59	0.90	1.33	7.44	0.01	0.09	0.11
MnO	b.d.l.		0.08					0.05				
MgO	3.50	13.32	11.43	0.61	0.49	1.00	3.22	3.58	27.32			
CaO	0.20	0.47	0.38		0.01		0.16	0.10	0.24	0.12	0.17	0.14
BaO	0.57	0.10	0.07	0.52	0.13	0.42	0.48	b.d.l.				
Na ₂ O	0.09	b.d.l.	0.08	0.56	0.48	0.12	0.34	0.22	0.01	11.76	11.65	11.39
K ₂ O	9.99	5.83	6.52	10.19	9.79	10.54	8.96	9.04	0.27	0.02		0.02
TOTAL	97.80	92.61	93.42	95.32	98.53	98.69	95.85	95.32	85.90	100.53	100.42	99.74
No oxygens	22	22	22	22	22	22	22	22	28	8	8	8
Si	6.928	5.963	6.189	6.032	6.282	6.532	6.669	6.744	5.38	2.993	2.992	2.995
Ti	0.013	0.021	0.013	0.290	0.009	0.020	0.031	0.028	0			
Al									–	1.009	1.009	1.010
Al iv	1.072	2.037	1.811	1.968	1.718	1.468	1.331	1.256	2.62			
Al vi	3.005	2.134	2.361	3.394	3.870	3.471	3.363	3.281	0.57			
Cr	0	0.013	0.023	0	0	0	0	0	0.02			
Fe ²⁺	0.419	0.430	0.341	0.217	0.082	0.388	0.098	0.146	3.89	0.000	0.003	0.004
Mn	0	0	0.009	0	0	0	0	0.005				
Mg	0.682	2.740	2.317	0.123	0.093	0.192	0.626	0.700	7.12			
Ca	0.027	0.069	0.056	0	0.001	0	0.022	0.014	0.04	0.006	0.008	0.007
Ba	0.029	0.005	0.004	0.027	0.006	0.021	0.024	0				

Table 1 – continued.

D. Chemical composition of the metamorphic sphalerite from samples WT-6601 (x1-x10) and Ang_St2 (x11-x12).

No.	x1	x2	x3	x4	x5	x6	x7	x8	x9	x10	x11	x12
Fe	2.42	2.25	2.29	2.09	2.16	2.01	2.02	2.25	2.18	2.44	1.65	1.41
Ni	0	0	b.d.l.	0	0	0	0	b.d.l.	0	b.d.l.	b.d.l.	b.d.l.
Cu	0	b.d.l.	0	0	0	0	0	0	0	0	0.37	1.18
Zn	65.38	65.65	65.34	65.23	65.12	65.10	64.22	64.94	64.37	64.54	65.26	62.76
Cd	b.d.l.	0.18	0.37									
Ag	0	b.d.l.	0	0	0	0	b.d.l.	0	0	b.d.l.	0	0
Pb	0	0	0	0	0	0	0	0	0	0	0	0
S	33.19	33.34	32.98	33.26	33.72	33.18	32.97	33.11	33.11	32.72	33.01	33.97
As	b.d.l.	0	0.38	0.59	0	0.38	0.65	0.71	2.00	0	b.d.l.	0.13
Se	b.d.l.	0	0	b.d.l.	b.d.l.	0	b.d.l.	b.d.l.	b.d.l.	0	b.d.l.	b.d.l.
TOTAL	100.99	101.25	100.99	101.18	100.99	100.67	99.86	101.02	101.67	99.71	100.47	99.82
kation contents on the basis of I (S+As)												
Fe	0.042	0.039	0.040	0.036	0.037	0.035	0.035	0.039	0.038	0.043	0.029	0.024
Ni	0	0	0	0	0	0	0	0	0	0	0	0
Cu	0	0	0	0	0	0	0	0	0	0	0.006	0.018
Zn	0.966	0.966	0.972	0.962	0.947	0.962	0.955	0.962	0.954	0.968	0.970	0.906
Cd	0	0	0	0	0	0	0	0	0	0	0.002	0.003
Ag	0	0	0	0	0	0	0	0	0	0	0	0
Pb	0	0	0	0	0	0	0	0	0	0	0	0
S	1	1	1	1	1	1	1	1	1	1	1	1
As	0	0	0.005	0.008	0	0.005	0.008	0.009	0.026	0	0	0.002
Se	0	0	0	0	0	0	0	0	0	0	0	0
X _{FeS}	4.15	3.86	3.95	3.62	3.74	3.49	3.55	3.90	3.82	4.25	2.88	2.56

Table 2

Orientations and statistical parameters of the means of NRM components identified in particular palaeomagnetic sites of Oscar II Land metacarbonates. Abbreviations: D – declination, I – inclination, S – total number of independently oriented hand samples collected and subjected to demagnetization procedures, s – total number of demagnetized cylindrical specimens, N/n – number of independently oriented hand samples/cylindrical specimens used for Fisher statistics, $\alpha_{95\%}$ – half angle of a cone of 95% confidence, κ – Fisherian precision parameter; in the separate column marked (+) is ChRM calculated using transposing procedure offered by Remasoft 3.0; bold are NRM components qualified for further tectonic interpretations; all parameters are presented for *in situ* orientation.

Site	Components	D (°)	I (°)	S/s	N/n	$\alpha_{95\%}$	κ	Transposing procedure	Increase of low field magnetic susceptibility
WTSJ1	WTSJ1L	210.7	50.7	5/11	4/8	80.9	1.43		from 425°C
	WTSJ1M	87	51.3	5/11	3/6	106	1.37	–	
WTSJ2	WTSJ2M	247.9	49.2	11/4	2/2	–	1.03	–	from 450°C
WTSJ3	WTSJ3M	23.9	14.9	7/18	3/6	49.1	2.81	–	from 400–500°C
WTSJ4	WTSJ4M	200.7	43.8	4/9	3/3	167.3	1.84	–	not recognized till 450°C
WTSJ5	WTSJ5M	100.7	-21.4	6/18	6/13	5.5	58.23	–	from 500°C
WTSJ6	WTSJ6L	200.7	46.8	8/19	8/18	31.3	2.20	–	after 200°C
	WTSJ6Ltr	166.3	49.1	8/19	8/18	23.3	3.17	+	
	WTSJ6M	182.8	78.9	8/19	6/11	79.4	1.30	–	
WTSJ7	WTSJ7M	77.6	30.3	7/16	4/8	72.1	1.55	–	from 450–500°C
	WTSJ7H	154.6	-34.9	7/16	2/3	83.4	3.28	–	
WTSJ8	WTSJ8M	84.4	-15.4	8/18	3/4	57.6	3.52	–	from 300°C
WTSJ9	WTSJ9M	59.8	-77.0	7/18	4/8	21.2	7.79	–	from 400–500°C
	WTSJ9H	29.2	-34.0	7/18	2/2	0.0	4.53	–	
WTENG10	WTENG10M	144.5	-18.8	6/18	2/7	29.8	5.06	–	from 425°C
WTENG11	WTENG11H	317.2	21.6	5/11	3/3	>90	1.44	–	not recognized till 680°C
WTENG12	WTENG12M	186.4	-46.9	5/14	2/5	17.9	19.18	–	not recognized till 400–450°C

the chemical equilibration of sphalerite with monoclinic pyrrhotite (with 4C superstructure) may give anomalously high pressure (Sangameshwar and Marshall 1980). It is evident that a more meaningful pressure estimate for the examined metacarbonates needs further mineralogical investigation.

Palaeomagnetic results

The NRM intensities of the investigated carbonates were found to be low ranging between 0.01–0.2 mA/m. The lower intensities (0.01–0.1 mA/m) were a characteristic feature of the sampled “pure” marbles (Type I of the investigated metacarbonates according to division in “Petrography of investigated metacarbonates”). The tectonised dark grey zones enriched in sulphides and graphite-like

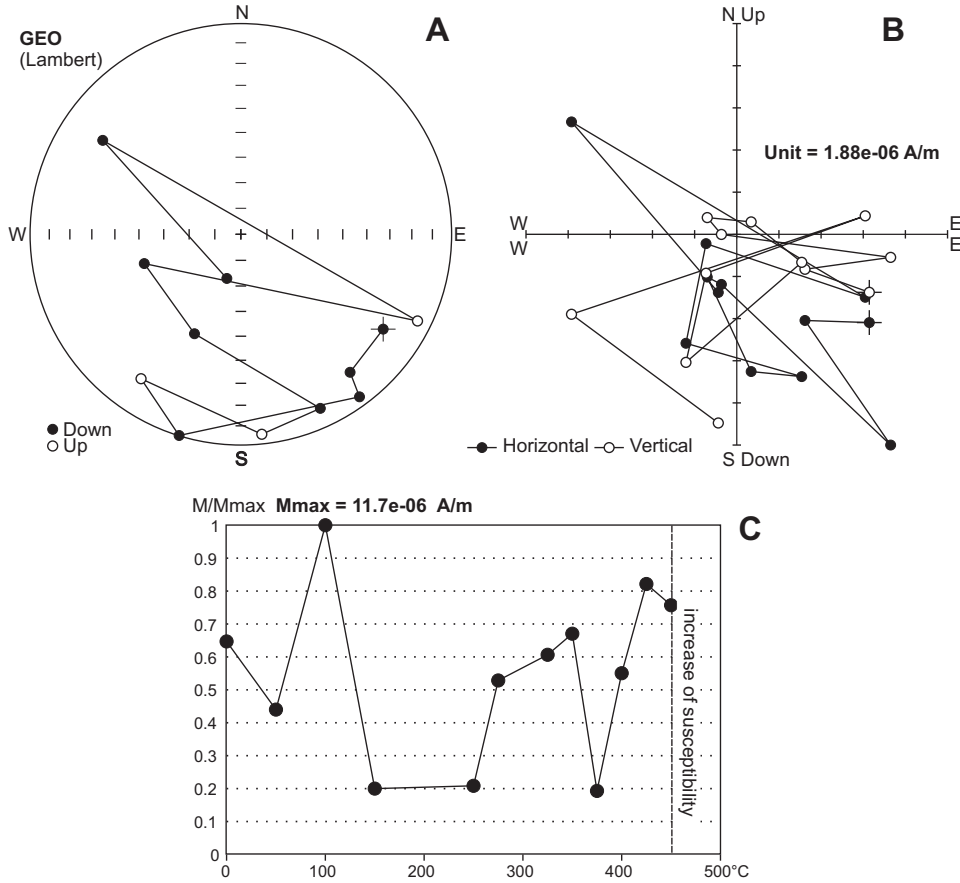


Fig. 11. Example of demagnetization diagrams of metacarbonates from the Western part of Oscar II Land – demagnetization behavior type I: equal area (A), orthogonal (Zijderveld) projections (B) and normalized intensity decay plots (C) of NRM during thermal demagnetization experiments; projections are presented for *in situ* orientation; on equal area projection open/full symbols represent upper/lower hemisphere; on orthogonal projection open/full symbols denote projections onto vertical/horizontal planes; other explanations are in the text.

substances where characterized by slightly higher intensities (0.1–0.2 mA/m). Approximately 80% of the specimens became unstable at 500°C.

In the course of the thermal demagnetization procedures three types of specimen behavior were recognized:

- Type I specimens rapidly became unstable from the first steps of demagnetizations (50–100°C). This kind of behavior was typical of specimens with NRM < 0.1 mA/m (Fig. 11).
- Type II specimens reveal a stable gradual demagnetization up to a temperature range of 400–500°C (a dominance of any of the ferromagnetic phases was not recognizable; Fig. 12).

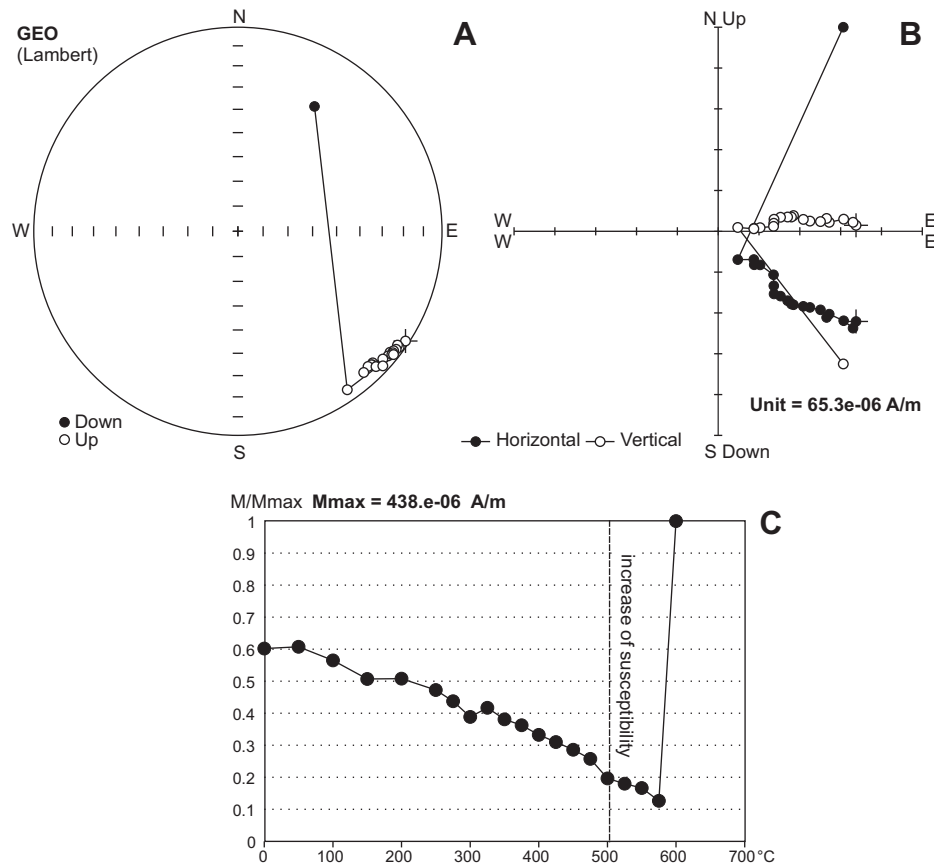


Fig. 12. Example of demagnetization diagrams of metacarbonates from the Western part of Oscar II Land – demagnetization behavior type II; other explanations are as in Fig. 11 and are in the text.

- Type III samples showed a stable demagnetization up to 250–300°C while a rapid demagnetization (“break down” of intensity by 80%) of the specimens took place between 300–350°C near to the $T_{ub \text{ max}}$ of pyrrhotite (Fig. 13).

The following CHRMs were identified in the samples:

- A low temperature component (index L) – $T_{ub} < 150^\circ\text{C}$, related to goethite, was recognized in sites WTSJ1 and WTSJ6,
- An intermediate temperature component (index M) – $T_{ub} = 150\text{--}350^\circ\text{C}$, related to pyrrhotite, was recognized in all sites except WTENG11,
- A high temperature component (index H) – $T_{ub} > 350^\circ\text{C}$, related to maghemite? and or hematite, was identified in sites WTSJ7, WTSJ9 and WTENG11.

In particular sites, the mean directions of NRM components were defined with varying precision and only one mean – WTSJ5M ($\alpha_{95\%} = 5.5^\circ$, $\kappa = 58.23$; Fig. 14, Table 2) passed the statistical criteria of “a well defined palaeomagnetic direction” described by Van der Voo (1993) – $\kappa > 10$, $\alpha_{95\%} < 16^\circ$. The following four means

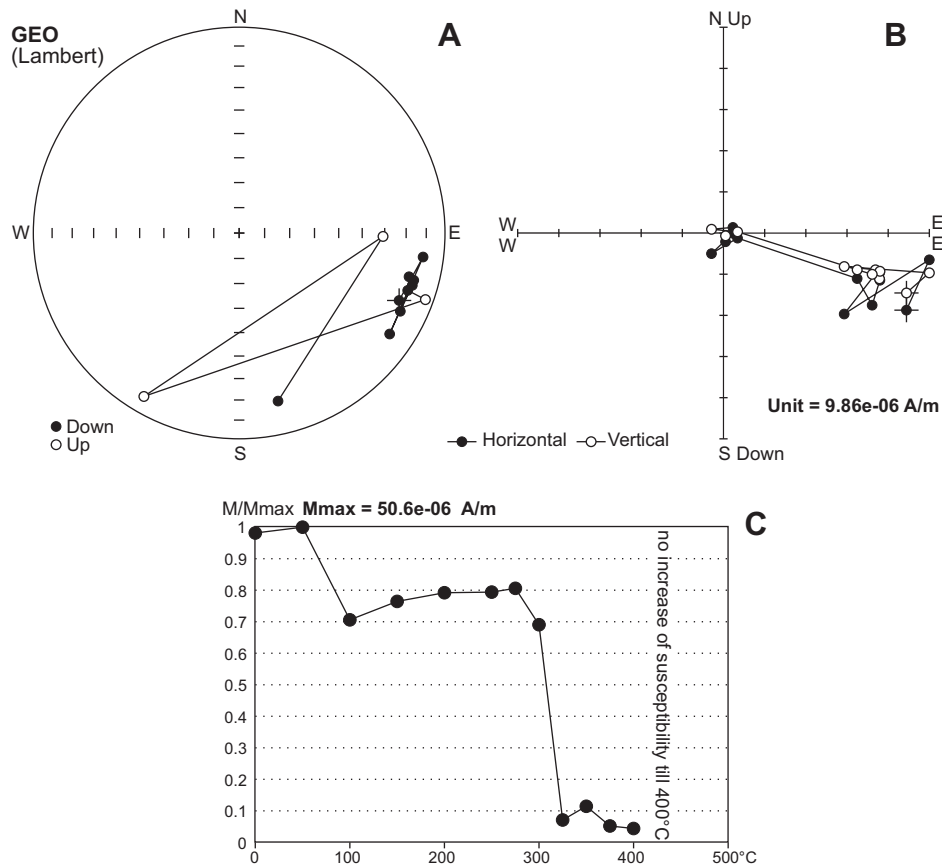


Fig. 13. Example of demagnetization diagrams of metacarbonates from the Western part of Oscar II Land – demagnetization behavior type III; other explanations are as in Fig. 11 and are in the text.

– WTSJ6Ltr, WTSJ9M, WTENG10M, WTENG12M with $\alpha_{95\%}$ not exceeding 30° were also used for further tectonic consideration (Fig. 14, Table 2). Site WTSJ6 low temperature directions are better grouped after applying transposing procedure offered by Remasoft 3.0 software which inverts part of the analyzed directions to achieve maximum clustering of the analyzed population (Table 2). This can suggest that the formation of the WTSJ6Ltr component could last long enough to record inversion of the ambient magnetic field. It should be stressed additionally that components WTENG10M and WTENG12M, although calculated from 7 and 5 specimens respectively, were identified in only 2 independently oriented hand samples in each of the sites. Twelve mean directions with $\alpha_{95\%} > 30^\circ$ were rejected from further analysis (Table 2).

The low-field magnetic susceptibility was closely monitored in the course of thermal demagnetization. The initial susceptibility of all the samples were low ranging from 10^{-4} to 10^{-5} SI. A diamagnetic behavior was observed in some of the samples. In the majority of sites a significant increase of susceptibility accompa-

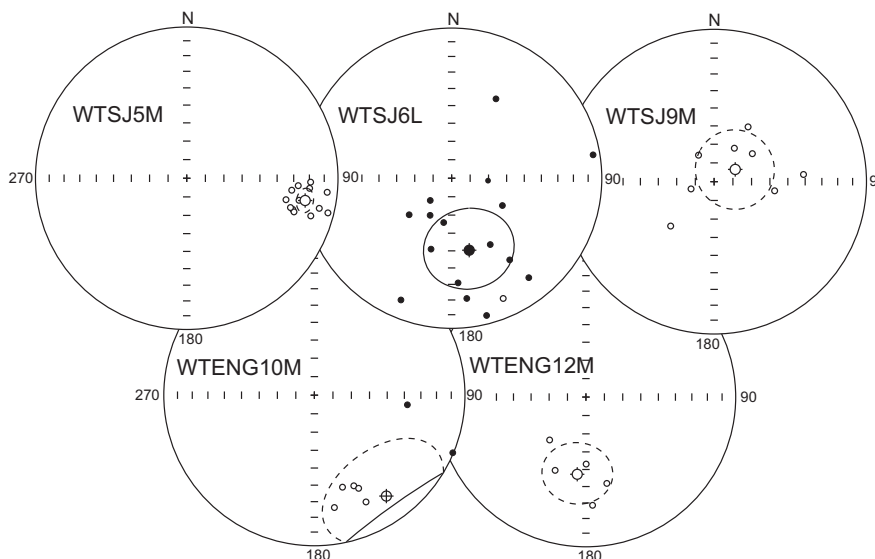


Fig. 14. Equal area projections of ChRM directions of 5 palaeomagnetic sites from Oscar II Land metacarbonates qualified for further tectonic interpretations; open/full symbols represent upper/lower hemisphere, site means are presented with their cones of $\alpha 95\%$ confidence. Orientations and statistical parameters of calculated means are presented in Table 2.

nied by an increase of the intensity and disturbance of the NRM structure of the specimens was noted around 400–500°C. This process may be the result of breakdown of pyrite to magnetite during thermal demagnetization. Although in the majority of sites it does not influence the extraction of L and M components it may have disturbed the proper definition of the H component. The exception to this was found for site WTSJ6 where the increase of susceptibility around 300°C enabled the extraction of only the L component.

It should be noted that only 51 of 181 demagnetized specimens qualified for further analysis. This can be, partially, due to the overlapping of temperature ranges for particular components, imprecise cleaning of the ChRMs, often an unstable NRM structure and low signal of the specimens. Partial scattering of the site directions can be related to post-magnetization tectonic (?) processes (*e.g.*, while the mean WTSJ7M is imprecisely defined – $\kappa = 1.55$, $\alpha 95\% = 72.1^\circ$ (Table 2), in specimens from site WTSJ7, the WTSJ7M component was calculated with a high precision – $ASD < 7^\circ$).

Interpretation of palaeomagnetic results in the light of tectonic structure of investigated area

The metacarbonates investigated in this study have been affected by polyphase deformation events. With the exception of the HP/LT Motalfjellet Group most of the

Caledonian rocks of Western Svalbard are interpreted to record intermediate pressure/temperature metamorphism (*cf.* Manby 1979, 1986; Morris 1988). Caledonian recrystallization and neomorphism began prior to and over-lapped the main highly ductile D1 deformation event. Large scale folds, which are often isoclinal, are characterized by a bedding parallel schistosity. The subsequent D2 event was also highly ductile with the F2 folds being near coaxial, tight to isoclinal structures so that the S1 and S2 foliations are often nearly parallel (Figs 4, 5). In contrast to the clearly metamorphic S1 foliation, the S2 fabric was developed by lower temperature diffusion mass transfer processes (pressure solution). Both D1 and D2 events were accompanied by the extensive carbonate and quartz veining systems reflecting the dewatering and fluid migration (and raised H₂O/CO₂ activities) within the affected lithologies. The resultant dehydration and complexity of the Caledonian deformation could have destroyed the primary “layer-cake” configuration of the rock succession decreasing its ability to develop, during the later West Spitsbergen Fold Belt event, a ramp-flat geometry like that found in the Late Palaeozoic–Mesozoic rocks to the east. Consequently, it is suggested here that the structural response to these later events by the already highly deformed and metamorphosed Caledonian rocks was essentially restricted to rigid blocks displacements. Thrust and later normal faulting were the main responses of these rocks to the WSFB deformation with the minor (F3–S3) folding concentrated along higher strain fault zones (Figs 4, 5). Some larger scale flexuring of the thrust slices and tightening of the Late Caledonian folds are also evident (*e.g.* Holmesletfjellet Syncline) where they have ascended listric bends in the floor thrusts.

Of the twelve sites sampled during the two field seasons only five qualified for further analysis. The most prospective of the sites sampled, site WTSJ5, was on the overturned western limb of the Holmesletfjellet syncline (Figs 2, 15). The mean WTSJ5M direction identified in site WTSJ5 exhibits an excellent grouping ($\alpha_{95\%} = 5.5^\circ$, $\kappa = 58.23$; Fig. 14, Table 2) and it is clearly imposed on the main Caledonian S1 fabric. The WTSJ5M *in situ* direction lies in the eastern sector of stereographic projection some distance from the palaeomagnetic directions of the Baltica reference path (Fig. 16). Pyrrhotite is the main ferromagnetic carrier in the

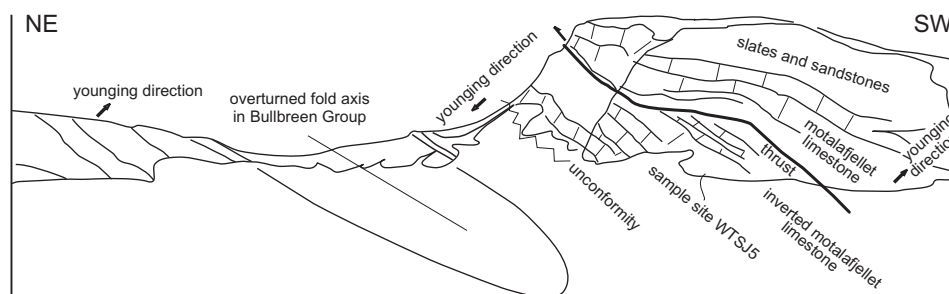


Fig. 15. Sketch of western Homlesletfjellet (view from NW, from Bullbreen Glacier). The location of the palaeomagnetic site WTSJ5 is also indicated.

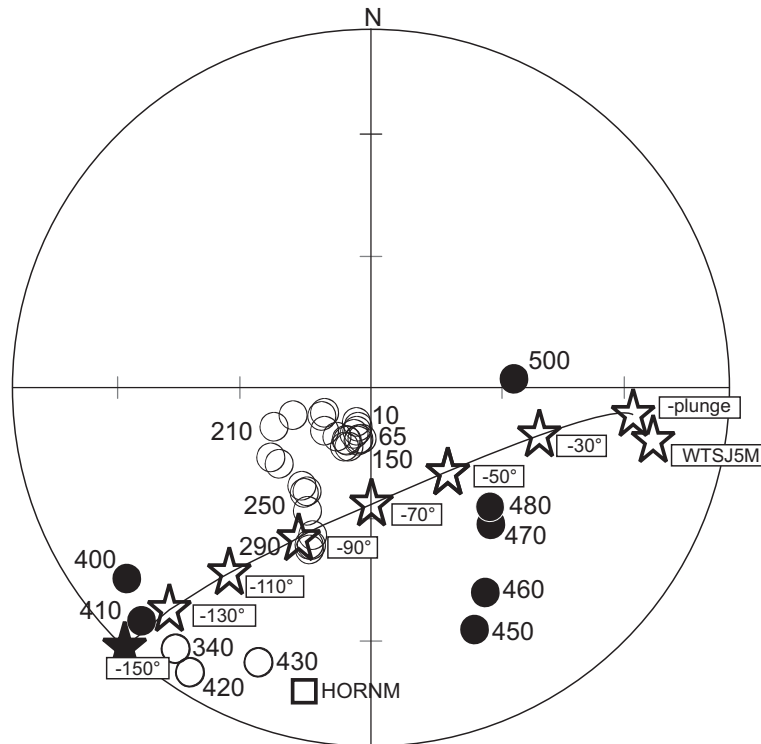


Fig. 16. Tectonic correction of palaeomagnetic result from site WTSJ5 – Holmesletfjellet syncline. Ovals represent palaeomagnetic directions recalculated from APWP of Baltica for mean West Oscar II Land location; ages of selected reference palaeomagnetic directions are given. The square indicates the expected orientation of Caledonian remagnetization identified in Hornsund (Michalski *et al.* 2012), recalculated from $HORN M_{VGP}$ palaeopole for West Oscar II Land. Stars represent orientation of WTSJ5M component *in situ* and in the following stages of tectonic correction; equal area projection; open/full symbols represent upper/lower hemisphere; The reference APWP of Baltica was derived from integral databases of GMAP 2012; other explanations are in the text.

samples from this site and it is convincingly of metamorphic (Caledonian) origin implying a possible 430–400 Ma metamorphic age for the WTSJ5 marbles. However, if WTSJ5M represents a post-folding Caledonian direction it would suggest a separation of the Western Svalbard Terrane from Baltica in Caledonian time. Although such a solution cannot be excluded it has not yet been confirmed by any other published palaeomagnetic data.

An alternative solution is that WTSJ5M is of Caledonian origin and it is rather a synfolding direction which was rotated by subsequently deformation event(s). The Holmesletfjellet Syncline axis plunges 12° toward 158° . After removing plunge of the axis and gradual unfolding around 158° WTSJ5M was seen to fall into the 290 Ma sector of the reference path (Fig. 16). Further unfolding by 40° shifts the WTSJ5M to the Silurian/Devonian sector of the reference path. This coincidence could suggest that initially a more open Caledonian syncline appears to have become

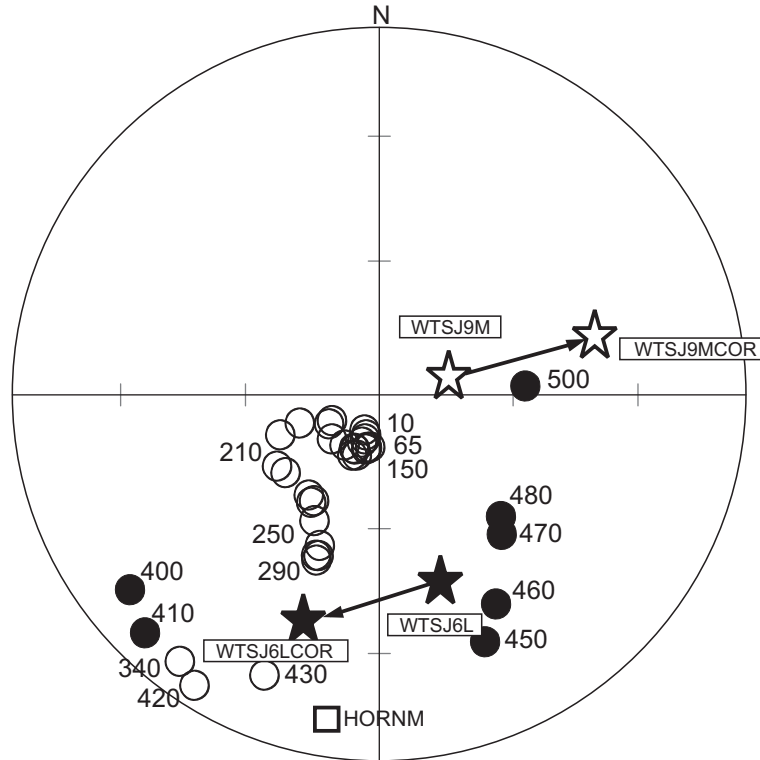


Fig. 17. Tectonic correction of palaeomagnetic results from sites WTSJ6 and WTSJ9 – S St. Jonsfjord. Stars represent orientation of identified components in *in situ* positions (labels WTSJ6L and WTSJ9M) and after reorientation of S1 schistosity in investigated sites to horizontal plane (labels WTSJ6LCOR and WTSJ9MCOR respectively); other explanations are as in Fig.16 and are in the text.

progressively refolded and overturned to the NE during the later stages of the main Caledonian deformation event or, more probably, during the Late Cretaceous–Paleogene West Spitsbergen Fold Belt event. The WTSJ5M direction may be, therefore, an equivalent of the HORN component of the Silurian Caledonian post-folding direction identified in Hornsund, which is part of the Central Svalbard Terrane (Michalski *et al.* 2012). Based on the similarity of the NRM structures and magnetic carriers of HORN and WTSJ5M such an interpretation is possible.

For sites WTSJ6 and WTSJ9, situated on the S shore of St. Jonsfjorden, a tectonic correction to the main S1 schistosity was applied to account for its rotation during the ascent on a listric floor thrust of the nappe containing these rocks during the E- to ENE-directed WSFB tectonic transport. The orientations of the main Caledonian schistosity averages 168/40S–165/35S in sites WTSJ6 and WTSJ9, respectively. WTSJ6L *in situ* is situated near the 480–450 Ma sector of the reference path while a tectonic correction towards the horizontal plane shifts this component in the direction of 410–400 Ma sector (Fig. 17). As this ChRM is carried by ferromagnetic phases with a $Tub < 150^\circ$ which indicates that it could have been influ-

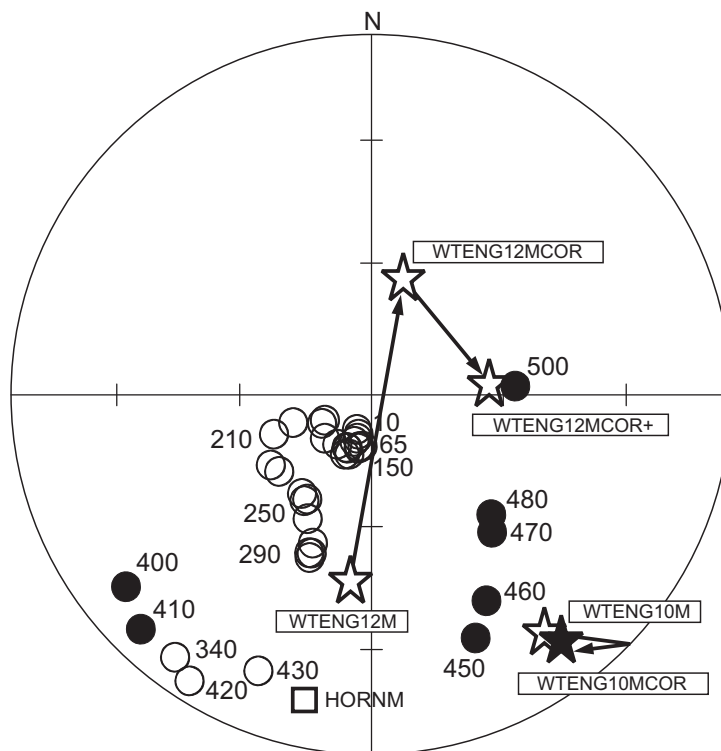


Fig. 18. Tectonic correction of palaeomagnetic results from sites WTENG10 and WTENG12 – Engelsbukta. Stars represent orientation of identified components in *in situ* positions (labels WTENG10M and WTENG12M) and after correction according to steepening of component rock orientations during ascent on floor thrusts (labels WTENG10M COR and WTENG12M COR respectively). In site WTENG12 additional correction for 70° anticlockwise tectonic rotation of Brøggerhalvøya with respect to dominant NNW-SSW tectonic trend of WSFB has been applied (star labeled WTENG12M COR+); other explanations are as in Fig. 16 and are in the text.

enced by recent magnetic field, a Palaeozoic age for this component is of low probability. It is likely that the direction is a composite artifact influenced by the dominance of goethite at site WTSJ6 which has been confirmed by three component IRM procedures (Lowrie 1990).

WTSJ9M *in situ* is situated near the 150–10 Ma sector of the reference path and the applied tectonic correction shifted the component away from that location in the ENE direction (Fig. 17). This could suggest that WTSJ9M is of post-tectonic origin which formed in Late Mesozoic–Paleogene time. Such a solution is, however, in conflict with the petrographic and rock-magnetic observations which suggest that “metamorphic” pyrrhotite is the main carrier of the identified intermediate temperatures components.

In the Engelsbukta area the general trend of thrusts changes dramatically from NNW-SSE south of the bay to WNW-ESE on Brøggerhalvøya (Fig. 3). Tectonic corrections for sites sampled in this area were applied to account for any

steepening of component rock orientations during ascent on floor thrusts. The thrusts affecting the sampled sites were oriented 172/65W on the south side of Engelskbukta at site WTENG10 and were oriented 100/70S at site WTENG12 on the north side of the bay. Additionally, in the case of WTENG12, a correction for possible anticlockwise rotation of Brøggerhalvøya tectonic structures with respect to the general NNW-SSE WSFB tectonic trend has been applied (correction has been applied by the angle of 70° around vertical axis; Fig. 18).

As the main carrier of the WTENG10M and WTENG12M signals is pyrrhotite it should be expected again that these components are of Caledonian age. Both components in *in situ* positions fall near the Palaeozoic sector of the reference path and applied tectonic correction according to the orientation of the thrusts and eventual horizontal anticlockwise rotation of Brøggerhalvøya tectonic structures moves them away from the expected Caledonian orientation (Fig. 18). This could suggest that in the area of Engelskbukta the influence of the Paleogene deformation on the geometry of Caledonian structures was minor. Such conclusion is not in accordance with the literature (*e.g.* Manby and Lyberis 1996; Bergh *et al.* 2000; Saalman and Theidig 2001, 2002) and our structural observations of the target area. This should be confirmed by a larger number of palaeomagnetic analyses and more statistically significant palaeomagnetic results.

It should be stressed that the area bordering Forlandsundet (the western part of Oscar II Land including St. Jonsfjorden, Engelskbukta and Prince Karls Forland) was subjected, in the Palaeogene time, to extensive normal faulting related to the formation of the Forlandsundet graben. If any of the related faults were of a listric character they could have been responsible for significant rotation of local strata around an axis parallel to the trend (NNW-SSW) of the graben bounding faults. Evaluation of such rotations, although they could significantly influence the palaeomagnetic directions obtained, was not attempted as data from seismic sections, for example, which could indicate the presence of such faults, are not available for the onshore sampling sites.

Conclusions

- Our structural observations, combined with those obtained from the literature, confirm the polyphase (Caledonide-WSFB) character of the deformation that has affected the investigated metacarbonates from Oscar II Land. The main low grade Caledonian schistosity (S1) accompanied the formation of large isoclinal (F1) folds of unknown vergence. These structures were refolded by widely developed ductile mesoscale (F2) folds which appear to also be of Caledonian origin. The D3, F3–S3 crenulation folds and cleavages are more localized structures and appear to be confined to high strain zones that are interpreted here to be of WSFB origin.
- The petrographic and mineralogical data obtained from the sampled rocks confirm that they record a greenschist facies metamorphic event. Optical/SEM thin

section analyses reveal extensive recrystallization and in many cases a spatial reorganization of minerals within all sampled metacarbonates. These analyses also show that in the course of metamorphism primary ferromagnetic minerals, including those of detrital and diagenetic origin, have been totally replaced by secondary ferromagnetic carriers. The latter are represented mainly by pyrrhotite and subordinate hematite/maghemite. The present mineralogical composition of ferromagnetic assemblages was controlled by: (I) a high activity of H₂O-CO₂-rich fluids expelled during greenschist facies metamorphism that enhanced oxygen fugacity leading to dissolution and/or breakdown of all primary Fe- and Fe-Ti oxides; (II) intensive replacement processes of primary magnetite (both Ti-free and Ti-bearing) by pyrite as a result of high activity of sulphur during metamorphism; and (III) a high organic matter content, recrystallized and thermally degraded during metamorphism that promoted contemporaneous growth of pyrrhotite-pyrite that was also responsible for the local protection of hematite/maghemite.

- Both mineralogical and rock magnetic experiments point to pyrrhotite as the most common ferromagnetic carrier. The mineralogical data obtained confirm the occurrence of monoclinic pyrrhotite with a 4C superstructure (Fe₇S₈) of ferromagnetic character. The complementary results of palaeomagnetic demagnetization reveal that in the majority of sampled sites the M component dominates with a T_{ub} = 150–350°C that is related to pyrrhotite. The observations of the spatial relations of the sulphides to metamorphic foliations and textural features such as the equigranular textures of the pyrite aggregates and the occurrence of calcite-quartz pressure-fringes around large rigid pyrite grains containing numerous pyrrhotite and sphalerite inclusions leave no doubt that pyrite-pyrrhotite association is of metamorphic origin. Other recognized ferromagnetic minerals including goethite, maghemite (?) and hematite have influenced the NRM structure of the samples to a lesser degree and were identified only in a few sites.
- From the integrated rock-magnetic-petrographic-mineralogical-palaeomagnetic investigations it is highly probable that the most stable common M palaeomagnetic component corresponds to the formation of pyrrhotite during the Caledonian metamorphism. However, a statistically significant site mean palaeomagnetic direction was obtained in only one of twelve sampled sites (site WTSJ5 – Holmesletfjellet Syncline). The basic question is which process caused the scattering of directions in the remaining eleven sites. In such weakly magnetized rocks (NRM intensities <0.2 mA/m) scattering can be partly explained by inaccurate thermal “cleaning” of particular ChRMs. Further, in such rocks even minor mineralogical changes caused by thermal heating can substantially influence the “fragile” structure of the NRM. The M component could be also locally disturbed by the brittle D3 Late Cretaceous–Paleogene WSFB deformation recognized in almost all investigated sites.
- WTSJ5M component recognized in the Western limb of Holmesletfjellet syncline reveals excellent grouping ($\alpha_{95\%} = 5.5^\circ$, $\kappa = 58.23$; Fig. 14, Table 2). Coin-

vidence of WTSJ5M with Silurian–Devonian sector of the Baltica reference path after unfolding of the syncline by the angle of 130° suggests synfolding origin of this direction. Our results suggest that after imposing of WTSJ5M which probably marks the final stages of Caledonian metamorphism (lowering of temperature, passing the rock through critical Curie points), the western limb of the Holmesletfjellet syncline has been refolded, that is, an originally open fold has been transformed into overturned syncline. There is still the question as to whether this fold reactivation could be related to the Late Caledonian shortening or was imposed in the Late Cretaceous–Paleogene time. Any further tectonic reconstructions in this area should be confirmed by palaeomagnetic fold tests procedures and additional sampling of both limbs of the Holmesletfjellet syncline.

Acknowledgements. — This study is part of the PALMAG project 2012–2015: *Integration of palaeomagnetic, isotopic and structural data to understand Svalbard Caledonian Terranes assemblage* funded by Polish National Science Centre (NSC) – grant number 2011/03/D/ST10/05193. Preliminary palaeomagnetic samples for this study were collected in 2006 in the course of the joint expedition of the Institute of Geophysics, Polish Academy of Sciences and University of Greenwich (United Kingdom) that was carried out along the Western and the Northern margins of Spitsbergen (Oscar II Land, Forlandsundet, Kongsfjord, Sorgfjord). The main palaeomagnetic sampling were undertaken in 2012 in the course of the palaeomagnetic expedition to Western Oscar II Land (St Jonsfjord and Engelsbukta) and Kongsfjord (Brøggerhalvøya and Blomstrandhalvøya) funded by the Polish NSC. Structural observations presented in this study are partly derived from structural data accumulated during a collaborative research program amongst Goldsmiths College (London), the Universities of Greenwich, Hamburg and Münster for the Brøggerhalvøya-Engelsbukta area (1985–1989) and from the CASE 1 project (Correlation of Arctic Structural Events – part 1: Spitsbergen, 1992). Structural data in all of the palaeomagnetic sampling sites were collected in 2006 and 2012. We are grateful to Prof. dr hab. Jerzy Nawrocki and Prof. dr hab. Stanisław Mazur for their critical reviews of this contribution and their many constructive comments. Finally, we would like to thank Aleksandra Hołda-Michalska for preparation of geological maps and improvements of the figures.

References

- BECKER M., DE VILLIERS J. and BRADSHAW D. 2010. The mineralogy and crystallography of pyrrhotite from selected nickel and PGE ore deposits. *Economic Geology* 105: 1025–1037.
- BERGH S.G. and ANDRESEN A. 1990. Structural development of the Tertiary fold-and-thrust belt in east Oscar II Land, Spitsbergen. *Polar Research* 8: 17–236.
- BERGH S.G., BRAATHEN A. and ANDRESEN A. 1997. Interaction of basement-involved and thin-skinned tectonism in the Tertiary fold-thrust belt of central Spitsbergen, Svalbard. *American Association of Petroleum Geologists Bulletin* 81: 637–661.
- BERGH S.G., MAHER H.D. and BRAATHEN A. 2000. Tertiary divergent thrust directions from partitioned transpression, Brøggerhalvøya, Spitsbergen. *Norsk Geologisk Tidsskrift* 80: 63–82.
- BERGH S.G., OHTA Y., ANDRESEN A., MAHER H.D., BRAATHEN A. and DALLMAN W.K. 2003. *Geological Map of Svalbard, 1: 100 000 sheet B8G St. Jonsfjorden*. Norsk Polarinstittutt Temakart No. 34.
- BUTLER R.F. 1992. *Paleomagnetism: Magnetic domains to geological terranes*. Blackwell Scientific Publications, Boston: 319 pp.

- CHADIMA M. and HROUDA F. 2006. Remasoft 3.0 – a user-friendly paleomagnetic data browser and analyzer. *Travaux Géophysiques* 27: 20–21.
- CHALLINOR A. 1967. The structure of Brøggerhalvøya, Spitsbergen. *Geological Magazine* 104: 322–336.
- DEKKERS M.J. 1989. Magnetic properties of natural pyrrhotite. II. High and low-temperature behaviour of Jrs and TRM as function of grain size. *Physics of the Earth and Planetary Interiors* 57 (3–4): 266–283.
- DUNLOP D.J. and ÖZDEMİR Ö. 1997. *Rock Magnetism Fundamentals and Frontiers*. Cambridge University Press, New York, London and Cambridge: 596 pp.
- FISHER R.A. 1953. Dispersion on a sphere. *Proceedings of the Royal Society of London* A217: 295–305.
- FROST B.R. 1991a. Stability of oxide minerals in metamorphic rocks. In: D.H. Lindsley (ed.) *Oxide minerals: Their petrologic and magnetic significance*. *Reviews in Mineralogy* 25: 469–487.
- FROST B.R. 1991b. Magnetic petrology: factors that control the occurrence of magnetite in crustal rocks. In: D.H. Lindsley (ed.) *Oxide minerals: Their petrologic and magnetic significance*. *Reviews in Mineralogy* 25: 489–509.
- HAGGERTY S.E. 1976. Opaque mineral oxides in terrestrial igneous rocks. In: Douglas III Rumble (ed.) *Oxide minerals*. *Reviews in Mineralogy* 3: Hg101–Hg300.
- HAGGERTY S.E. 1991. Oxide textures – A mini-atlas. In: D.H. Lindsley (ed.) *Oxide minerals: Their petrologic and magnetic significance*. *Reviews in Mineralogy* 25: 129–219.
- HARLAND W.B. 1997. The Geology of Svalbard. *Geological Society of London. Memoir* 17: 521 pp.
- HARLAND W.B. and WRIGHT N.J.R. 1979. Alternative hypothesis for the pre-Carboniferous evolution of Svalbard. *Norsk Polarinstitutt Skrifter* 167: 89–117.
- HINKE A. 1989. *Geologische Karte des kristallins der Brøggerhalvøya unpublished map*. Geologische Paläontologischen Institut, Universität Hamburg.
- HIRAJIMA T., BANNO S., HIROI Y. and OHTA Y. 1988. Phase petrology of eclogites and related rocks from the Motalafjella high-pressure metamorphic complex in Spitsbergen (Arctic Ocean) and its significance. *Lithos* 22: 75–97.
- HJELLE A., PIEPJOHN K., SAALMANN K., OHTA Y., SALVIGSEN O., THIEDIG F. and DALLMANN W. 1999. *Geological map of Svalbard 1:100 000, sheet A7G Kongsfjorden*. Norsk Polarinstitutt Temakart No. 30.
- JELEŃSKA M. and LEWANDOWSKI M. 1986. A palaeomagnetic study of Devonian sandstone from Central Spitsbergen. *Geophysical Journal of the Royal Astronomical Society* 87: 617–632.
- KANAT L.H. 1985. *Aspects of the Geology of Southwest Oscar II Land, Spitsbergen*. Unpublished PhD thesis, University of Cambridge, Cambridge: 253 pp.
- KIRSCHVINK J. 1980. The least square line and plane and analysis of paleomagnetic data. *Geophysical Journal of the Royal Astronomical Society* 62: 699–718.
- KONTNY A., DE WALL H., SHARP T.G. and PÓSFAL M. 2000. Mineralogy and magnetic behavior of pyrrhotite from a 260°C section at the KTB drilling site, Germany. *American Mineralogist* 85: 1416–1427.
- LABROUSSE L., ELVEVOLD S., LEVRIER C. and AGARD P. 2008. Structural analysis of high-pressure metamorphic rocks of Svalbard: Reconstructing the early stages of the Caledonian orogeny. *Tectonics* 27 (5): TC5003.
- LOSKE B. 1989. *Geologische kartierung 1:10,000 der westlichen Bereich der Trondheimfjellet und des Bull-Simonsfjella und untersuchung an tectonischen structuren in mehr deformierten gesteinen des Hekla Hoek Komplexes in Nordwestern des Oscar II landes, Westspitbergen, Svalbard, Norwegen*. Diplom. Arbeit., University Münster, Münster: 114 pp. (unpublished).
- LOWRIE W. 1990. Identification of ferromagnetic minerals in a rock by coercivity and unblocking temperature properties. *Geophysical Research Letters* 17: 159–162.
- LUPTÁK B., JANÁK M., PLAŠIENKA D. and SUSANNE S.T. 2003. Alpine low-grade metamorphism of the Permian–Triassic sedimentary rocks from the Veporic Superunit, Western Carpathians – phyllosilicate composition and “crystallinity” data. *Geologica Carpathica* 54: 367–375.

- LUSK J. and FORD C.E. 1978. Experimental extension of the sphalerite geobarometer to 10 kbar. *American Mineralogist* 63: 516–519.
- LYBERIS N. and MANBY G.M. 1993. The origin of the West Spitsbergen Fold Belt from geological and plate kinematics: implications for the Arctic. *Tectonophysics* 224: 371–391.
- MANBY G.M. 1979. *Geology of North Prins Karls Forland, Svalbard*. Unpublished PhD thesis, University of Cambridge, Cambridge: 232 pp.
- MANBY G.M. 1986. Mid-Palaeozoic metamorphism and polyphase deformation of the Forland Complex, Svalbard. *Geological Magazine* 123: 651–663.
- MANBY G.M. and LYBERIS N. 1996. State of stress and the tectonic evolution of the West Spitsbergen Fold Belt. *Tectonophysics* 267: 1–29.
- MANBY G.M. and LYBERIS N. 2001. Emergence of Basement Dominated Nappes in Oscar II Land: Implications for Shortening Estimates. *Geologisches Jahrbuch B91*: 109–125.
- MARTÍN J.D. and GIL A.S.I. 2005. An integrated thermodynamic mixing model for sphalerite geobarometry from 300 to 850°C and up to 1 GPa. *Geochimica et Cosmochimica Acta* 69: 995–1006.
- MICHALSKI K. and LEWANDOWSKI M. 2004. Palaeomagnetic results from the Middle Carboniferous rocks of the Hornsund region, southern Spitsbergen: preliminary report. *Polish Polar Research* 25 (2): 169–182.
- MICHALSKI K., LEWANDOWSKI M. and MANBY G.M. 2012. New palaeomagnetic, petrographic and ⁴⁰Ar/³⁹Ar data to test palaeogeographic reconstructions of Caledonide Svalbard. Cambridge University Press. *Geological Magazine* 149 (4): 696–721.
- MORIMOTO N., GYOBU A., MUKAIYAMA H. and IZAWA E. 1975. Crystallography and stability of pyrrhotites. *Economic Geology* 70: 824–833.
- MORRIS A.P. 1988. Polyphase deformation in Oscar II Land, central western Svalbard. *Polar Research* 6: 69–84.
- NAWROCKI J. 1999. Paleomagnetism of Permian through Early Triassic Sequences in central Spitsbergen: implications for paleogeography. *Earth and Planetary Science Letters* 169: 59–70.
- PIEJOHN K., THIEDIG F. and MANBY G.M. 2001. Nappe stacking on Brøggerhalvøya, NW Spitsbergen. *Geologisches Jahrbuch B91*: 55–79.
- POWELL A.V., VAQUEIRO P., KNIGHT K.S., CHAPON L.C. and SANCHEZ R.D. 2004. Structure and magnetism in synthetic pyrrhotite Fe₇S₈: a powder neutron-diffraction study. *Physical Review B* 70: 014415-1–014415-12.
- SAALMANN K. and THIEDIG F. 2001. Tertiary West Spitsbergen fold and thrust belt on Brøggerhalvøya, Svalbard: Structural evolution and kinematics. *Tectonics* 20 (6): 976–998.
- SAALMANN K. and THIEDIG F. 2002. Thrust tectonics on Brøggerhalvøya and its relationship to the Tertiary West Spitsbergen Fold and Thrust Belt. *Geological Magazine* 139 (1): 47–72.
- SANGAMESHWAR S.R. and MARSHALL B. 1980. Sphalerite geobarometry of deformed sulphide ores from the C.S.A Mine, Cobar, Australia. *Mineralium Deposita* 15: 305–314.
- SCOTT S.D. 1973. Experimental calibration of the sphalerite geobarometer. *Economic Geology* 68: 466–474.
- TOKONAMI M., NISHIGUCHI K. and MORIMOTO N. 1972. Crystal structure of a monoclinic pyrrhotite (Fe₇S₈). *American Mineralogist* 57: 1066–1080.
- WELBON A.I. and MAHER H.D. 1992. Tertiary tectonism and basin inversion of the St Jonsfjorden region, Svalbard. *Journal of Structural Geology* 14: 41–55.
- VAN DER VOO R. 1993. *Paleomagnetism of the Atlantic, Tethys and Iapetus Oceans*. Cambridge University Press, Cambridge: 424 pp.

Received 10 September 2014

Accepted 24 November 2014